

Hall-Effect Thruster Simulations with 2-D Electron Transport and Hydrodynamic Ions

IEPC-2009-114

*Presented at the 31st International Electric Propulsion Conference,
University of Michigan • Ann Arbor, Michigan • USA
September 20 – 24, 2009*

Ioannis G. Mikellides,^{*} Ira Katz,[†] Richard H. Hofer[‡] and Dan M. Goebel[§]
Jet Propulsion Laboratory, California Institute of Technology, Pasadena, CA, 91109

Abstract: A computational approach that has been used extensively in the last two decades for Hall thruster simulations is to solve a diffusion equation and energy conservation law for the electrons in a direction that is perpendicular to the magnetic field, and use discrete-particle methods for the heavy species. This “hybrid” approach has allowed for the capture of bulk plasma phenomena inside these thrusters within reasonable computational times. Regions of the thruster with complex magnetic field arrangements (such as those near eroded walls and magnets) and/or reduced Hall parameter (such as those near the anode and the cathode plume) challenge the validity of the quasi-one-dimensional assumption for the electrons. This paper reports on the development of a computer code that solves numerically the 2-D axisymmetric vector form of Ohm’s law, with no assumptions regarding the rate of electron transport in the parallel and perpendicular directions. The numerical challenges related to the large disparity of the transport coefficients in the two directions are met by solving the equations in a computational mesh that is aligned with the magnetic field. The fully-2D approach allows for a large physical domain that extends more than five times the thruster channel length in the axial direction, and encompasses the cathode boundary. Ions are treated as an isothermal, cold (relative to the electrons) fluid, accounting for charge-exchange and multiple-ionization collisions in the momentum equations. A first series of simulations of two Hall thrusters, namely the BPT-4000 and a 6-kW laboratory thruster, quantifies the significance of ion diffusion in the anode region and the importance of the extended physical domain on studies related to the impact of the transport coefficients on the electron flow field.

Nomenclature

\mathbf{B} = magnetic induction field	ΔA = surface area of a finite-element edge
\mathbf{c} = particle thermal (or random) velocity	Δt = time increment
\mathbf{E} = electric field	$\boldsymbol{\varepsilon}$ = contributions to Ohm’s law from the electron pressure and ion current density
e = electron charge	ε_0 = permittivity in vacuum
\mathbf{F}_i = total specific force on ions	ε_s = ionization potential of species “s”
f_i = ion velocity distribution function	η = total or effective electrical resistivity
$(\dot{f}_i)_c$ = rate of change of f_i due to collisions with other species	η_{ei} = electron-ion (e-i) electrical resistivity

^{*} Member of the Technical Staff, Electric Propulsion Group, Ioannis.G.Mikellides@jpl.nasa.gov.

[†] Group Supervisor, Electric Propulsion Group, Ira Katz@jpl.nasa.gov.

[‡] Member of the Technical Staff, Electric Propulsion Group, Richard.H.Hofer@jpl.nasa.gov.

[§] Section Staff, Propulsion and Materials Engineering Section, Dan.M.Goebel@jpl.nasa.gov.

$\mathbf{j}_{i(e)}$ = ion (electron) current density
 k_B = Boltzmann's constant
 L = length of the acceleration channel
 $\ln(\Lambda)$ = coulomb logarithm
 $m_{i(e)}$ = mass of ion (electron)
 $n_{i(e)}$ = number density of ion (electrons)
 n_n = number density of atoms (neutrals)
 $\hat{\mathbf{n}}$ = normal unit vector
 \dot{n} = ionization rate
 $p_{i(e)}$ = ion (electron) pressure
 q_i = ion charge (eZ)
 Q^T = thermal heating
 $\mathbf{R}_{i(e)}$ = ion (electron) drag force density
 r, z = radial and axial coordinates
 $\hat{\mathbf{r}}, \hat{\mathbf{z}}$ = unit vectors in radial and axial directions
 $T_{i(e)}$ = ion (electron) temperature
 t = time
 $\mathbf{u}_{i(e)}$ = mean velocity of ions (electrons)
 \mathbf{u}_n = mean velocity of atoms
 $u_{T,i}$ = ion thermal speed $(2k_B T_i / m_i)^{1/2}$
 \mathbf{v} = particle velocity
 Z = ion charge state

Greek Symbols

α = Bohm collision-rate factor
 $\hat{\mathbf{b}}$ = magnetic induction field unit vector
 $\beta_{r(z)}$ = r (z) component of magnetic induction field unit vector

η_0 = classical electrical resistivity
 κ_e = electron thermal conductivity
 λ_{ii} = ion-ion collision mean free path
 λ_{in} = ion-neutral charge-exchange collision mean free path
 μ_0 = classical electron mobility
 ν_B = Bohm collision rate
 ν_{ei} = electron-ion (e-i) collision rate
 $\bar{\nu}_{ei}$ = total electron-ion (e-i) collision rate
 ν_{en} = electron-neutral (e-n) collision rate
 ν_{en}^I = electron-neutral (impact) ionization rate
 ν_{ew} = electron-wall (e-wall) collision rate
 ν_{ew} = electron-wall (e-wall) collision rate
 ν_{is} = collision rate of ions with species "s"
 σ_{in} = ion-neutral charge-exchange collision cross-section
 τ_e = coulomb collision relaxation time for electrons
 τ_{ei}^T = thermal equilibration time between electrons
 τ_i = coulomb collision relaxation time for ions
 ϕ = plasma potential
 χ = magnetic-field potential function
 ψ = magnetic-field stream function
 ω_{ce} = electron cyclotron frequency

I. Introduction

THE numerical simulation of Hall thrusters spans more than two decades. In fact, the first theoretical models of the partially-ionized gas in Stationary Plasma Thrusters (SPT) were proposed in the early 1960s by Morozov and colleagues.^{1,2,3} Hirakawa^{4,5,6} developed one of the first numerical models of an SPT in three-dimensions. Electrons and singly-charged ions were simulated using a Particle-In-Cell (PIC) scheme that was combined with a Monte-Carlo Collision model (MCC). The electric field was determined by solving Poisson's equation. A computational approach that has been used extensively in the last two decades or so to simulate the partially-ionized gas in Hall thrusters is to solve the inertia-less fluid momentum and energy conservation laws for the electrons but use discrete-particle methods to track the evolution of the heavy species. This "hybrid" approach has allowed for the capture of bulk plasma phenomena in the thruster within reasonable computational times, and has therefore gained considerable popularity in the U.S and Europe. One of the first models to follow this approach was developed by Fife and Martínez-Sánchez.⁷ The model, dubbed "HPHall" (Hybrid-PIC Hall), uses a PIC-MCC method for ions in 2-D axisymmetric geometry and it appears that it was the first to reproduce the so-called breathing mode oscillations in Hall thrusters.⁸ A model for anomalous electron mobility was employed in the original (SPT-70) simulations with a scaling that was based on Bohm's scaling⁹ for the anomalous (or neoclassical) collision rate $\nu_B \sim B/16$. The precise numerical value used in the simulations was guided by experiments. Since the late 90s HPHall has been used to simulate several other thrusters and, naturally, its numerical and physical models have undergone several improvements and extensions. Recently the model was upgraded to HPHall-2** by Parra and Ahedo.¹⁰ Additional algorithm augmentations including an erosion sub-model were completed at JPL.^{11,12,13} A similar hybrid approach has been followed by Fernandez and Cappelli that led to the development of a similar model of Hall thrusters and is reported in Refs 14,15. Hagelaar, *et. al.*^{16,17} also followed a hybrid approach but instead of Bohm diffusion used empirical parameters to account for additional anomalous electron transport and energy loss phenomena. It is

** All simulation results presented in this paper that are termed as "HPHall" results were in fact generated with the HPHall-2 version of the code.

interesting to note that despite the apparent popularity of the hybrid approach in recent years, the earliest attempts to model the heavy species followed purely hydrodynamic formalisms¹⁸ (also reported in Ref. 19). A hydrodynamic approach for all species in the thruster was also applied later in 2-D geometries by Keidar and Boyd.²⁰

Because the fundamental principle behind the acceleration of ions in Hall thrusters is based on operating the accelerator at high electron Hall parameter ($\Omega_e \gg 100$), the diffusion of heat and mass for the electron flow in the direction parallel to the magnetic field is much greater (by $\sim \Omega_e^2$) than that in the perpendicular direction for most of the channel region. This leads to a simplification, the so-called quasi-one-dimensional approximation: streamlines of the magnetic vector field are also lines of constant electron temperature and constant “thermalized” potential $\phi^* \equiv \phi - T_e \ln(n_e)$. Numerically, the assumption allows for the solution of the plasma potential and electron temperature in a (quadrilateral) computational cell that is bounded by two adjacent lines of force rather than one with arbitrary dimensions. This is the approach followed in HPHall. Modeling regions of the thruster with complex magnetic field arrangements (such as those near eroded walls and magnets) and/or reduced Hall parameter (such as those near the anode and the cathode plume) challenge the validity of the quasi-one-dimensional assumption for the electrons.

In this paper we present a 2-D computational model of the partially-ionized gas in a Hall thruster that employs the full vector form of Ohm’s law, with no assumptions regarding the rate of electron transport in the parallel versus the perpendicular direction of the magnetic field. The model is a descendant of OrCa2D, a 2-D computational model of electric propulsion hollow cathodes that employs a mix of implicit and explicit algorithms to solve numerically the conservation laws for the partially-ionized gas in these devices.^{21,22} Numerical diffusion due to the large disparity of the transport coefficients in the two directions is evaded by solving the equations in a computational mesh that is aligned with the magnetic field. The use of field-aligned meshes for the simulation of highly-anisotropic plasmas is not uncommon, especially in the fusion energy community. Field-aligned meshes have been attempted in electric propulsion as well, to simulate processes in ion engine discharge chambers.²³ The fully-2D approach followed here allows for a large physical domain that extends more than five times the thruster channel length in the axial direction, and encompasses the cathode boundary. The main motivation is to extend the solution to regions of the Hall thruster that otherwise could not be modeled accurately due to the quasi-1D assumption. The model also incorporates a new algorithm for the solution of the (collisionless) neutral gas density, based on line-of-sight formulations, that eliminates the inherent statistical fluctuations of conventional particle methods. The approach for the neutral gas is presented in a companion paper²⁴ and will not be described here. The ions are modeled using a fully hydrodynamic approach that, in addition to the inelastic collision terms associated with the ionization, retain both the ion pressure and the ion-neutral charge-exchange “drag” term in the momentum equation.

The paper is organized as follows. Section II provides a description of the physical models and numerical methodologies for the ions (II.A) and electrons (II.B). Section III presents results from numerical simulations of two thrusters, namely the BPT-4000 and a 6 kW laboratory Hall thruster. The numerical simulations of the BPT-4000 (III.A) have been performed mainly for benchmarking purposes and the results are compared with those from recent HPHall simulations of the same thruster. Preliminary studies to better understand the impact of the imposed Bohm collision rate in the BPT-4000 benchmark simulations motivated an extended investigation in the 6 kW laboratory thruster; the results from these studies are presented in III.B. For the sake of brevity when comparing results with those from HPHall we refer to the newly-developed model as “Hall 2De.”

II. The Computational Model

The computational region in Hall 2De extends several channel lengths (L) downstream of the thruster exit. A schematic of the physical domain with naming conventions for the various boundaries are provided in Figure 1. The typical extent of the computational region in an HPHall simulation is also shown for comparison. Ions are treated as an isothermal, cold (relative to the electrons) fluid, accounting for charge-exchange and multiple-ionization collisions in the momentum equations. Although electron-impact collisions that lead to the ionization of an atom can be frequent by comparison to its transit time inside the channel, for most Hall thrusters, collisions between the atomic species (“neutrals”) are rare. A popular numerical method for simulating the flow of neutrals in Hall thrusters is PIC combined with DSMC to account for ionization collisions. An inherent disadvantage of particle methods like PIC is the noise that is generated due to the particle statistics, which can be reduced by including more particles but at the expense of increased computation time. The method followed in Hall 2De is based on widely-used methods to model problems such as photon transport in radiation heat transfer problems⁶ and is advancement over a previous algorithm that has been used to model regions of collisionless flows in electric propulsion hollow cathodes.^{21,22} The method assumes that particles striking a surface are fully accommodated and that the fraction of those particles that

is re-emitted follows a cosine distribution. The particle flux on any given surface depends then on the view factor between that surface and all other surfaces that emit particles. Because the basis for computing particle distributions in a region bounded by emission surfaces are the view factors the problem then becomes essentially a problem in geometry. The view factors can be computed at the pre-processing phase of the simulation thereby contributing an insignificant amount to the total computation time. The approach for the neutral gas is presented in a companion paper²⁴ and will not be described here. A 2-D form of Ohm's law and the electron energy equation are solved for the electrons and the equations are discretized on a field-aligned computational mesh. Ohm's law is combined with the current conservation equation to yield the plasma potential. The boundary conditions related to the sheath along the dielectric walls, and conditions for the remaining boundaries are provided in ensuing sections.

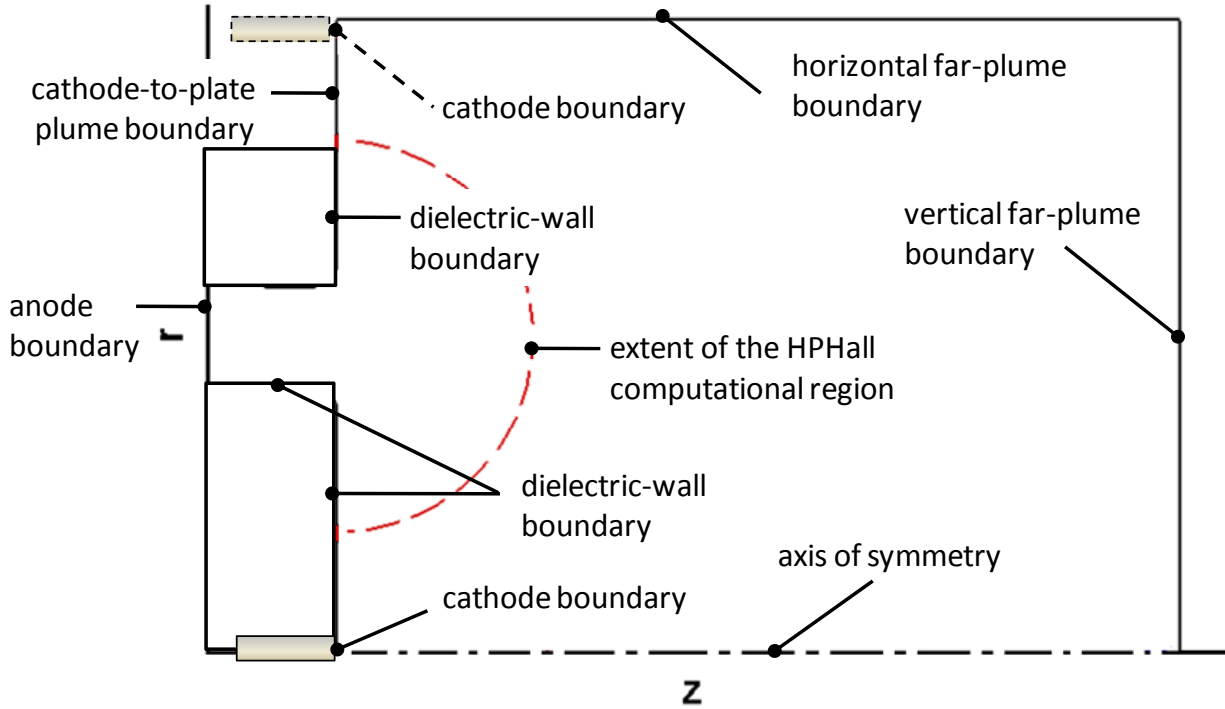


Figure 1. Schematic of the computational region and naming conventions for the boundary conditions.

A. Ions

1) Physics model

Because the treatment of ions, specifically the computational methods employed to determine their evolution inside the acceleration channel, has been wide-ranging due largely to the assumptions made on their characteristic collision scales, it is worth outlining estimates of the relevant characteristic sizes for the ions with some more detail. The two characteristic times for relaxation to a fluid, τ_e and τ_i of electrons and ions respectively are (with temperature expressed in K):

$$\tau_e = \langle v_{ei} \rangle^{-1} = \frac{3(2\pi)^{3/2} \epsilon_0^2 \sqrt{m_e} (k_B T_e)^{3/2}}{n_i Z^2 e^4 \ln \Lambda} \quad (\text{II-1})$$

$$\tau_i = \langle v_{ii} \rangle^{-1} = \frac{12\pi^{3/2} \epsilon_0^2 \sqrt{m_i} (k_B T_i)^{3/2}}{n_i Z^4 e^4 \ln \Lambda} = \left(\frac{2m_i}{m_e} \right)^{1/2} \left(\frac{T_i}{T_e} \right)^{3/2} \frac{\tau_e}{Z^2}$$

Hereon, our convention will exclude the brackets from mean values of the collision rate, that is $\langle v \rangle \equiv v$. For slow-moving ions the (Spitzer) thermal equilibration time between singly-charged ions and electrons when $T_i \leq T_e$ may be approximated by

$$\tau_{ei}^T \approx \frac{m_i}{2m_e} \tau_e \quad (\text{II-2})$$

Using estimated values in the 6 kW laboratory Hall thruster, the ion transit time $\tau_u=L/u_i$ can range approximately from $\sim(0.03 \text{ m})/(2 \times 10^4 \text{ m/s})=1.5 \text{ } \mu\text{s}$ for those ions that are accelerated downstream of the channel to $\sim(0.01 \text{ m})/(5 \times 10^2 \text{ m/s})=10 \text{ } \mu\text{s}$ for those generated near the anode region and lost to the walls. In comparison, the thermal equilibration time ranges between 0.03-0.5 sec. in the channel. This implies that the ions remain “cold” relative to the electrons. The (thermal) mean-free-path (mfp) for ion-ion collisions

$$\lambda_{ii} \approx u_{T,i} \tau_i, \quad (\text{II-3})$$

is plotted in Figure 2-left along the middle of the acceleration channel of the 6 kW Hall thruster for various (assumed) values of the ion temperature. The profiles have used the HPHall-computed values¹³ for the plasma density and electron temperature. It will be shown later that the ion density may in fact be substantially higher in the anode region than the values predicted by HPHall, which would suggest even smaller collision mfps for ions in this region than those plotted in Figure 2-left. Also, recent Laser-Induced Fluorescence measurements of Xe^+ inside the 6 kW Hall thruster suggest that ions follow very closely the equilibrium distribution function.²⁵ Figure 2-right depicts the charge-exchange collision mfp for ions with neutrals as estimated by,

$$\lambda_{in} \approx (\sigma_{in} n_n)^{-1}, \quad (\text{II-4})$$

and is plotted for two values of the charge-exchange cross-section σ_{in} : $50 \text{ } \text{\AA}^2$ and $100 \text{ } \text{\AA}^2$. Based on the measurements of Miller *et. al.*,²⁶ the two values cover the range of typical ion energies attained in the channel, $<1 \text{ eV}$ to 300 eV , with the higher value of the cross-section representing the lowest-energy ions. For comparison, the characteristic mfp for self collisions between neutrals, $\lambda_{nn} \approx (\pi n_n D^2 \sqrt{2})^{-1}$ is also plotted in Figure 1-right using a mean atomic diameter for xenon of $D=2.6 \text{ } \text{\AA}$.²⁷

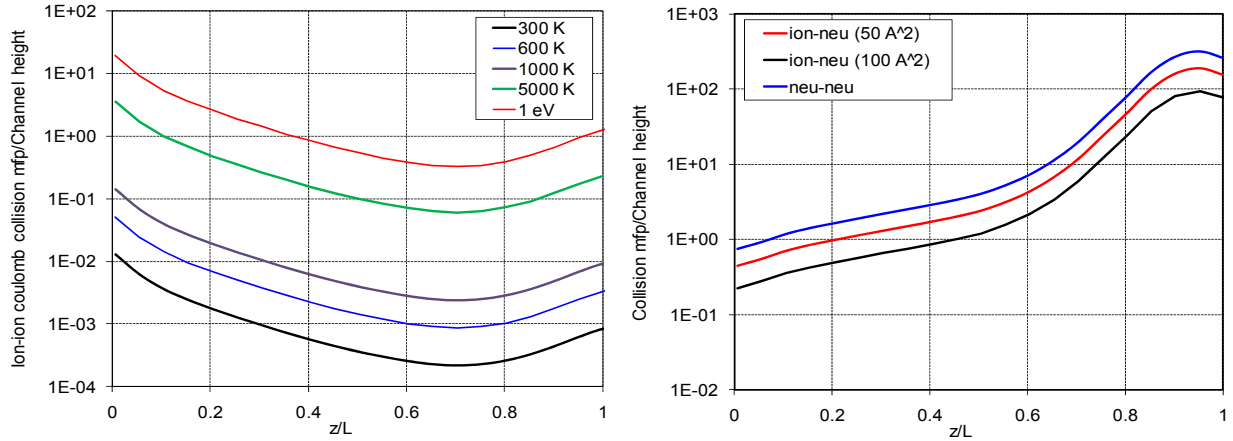


Figure 2. Collisions mean free paths at the middle of the acceleration channel in the 6 kW laboratory Hall thruster. Left: Ion-ion coulomb collisions for different values of the ion temperature. Right: Ion-neutral charge-exchange and neutral-neutral collisions.

Based on the estimates in Figure 2 the approach followed here is to treat ions as a fluid, and include charge-exchange collisions as a contribution to the (elastic) friction or “drag” force, whereas neutrals will be simulated using a collisionless approach.²⁴ It is noted that the addition of charge-exchange collisions can become increasingly important in the anode region since the electric force can be negligibly small there as by suggested by recent measurements of the plasma potential.²⁸

The formulations that lead to the momentum conservation law begin with Boltzmann’s equation for the distribution function of ions $f_i(t, \mathbf{r}, \mathbf{v})$

$$\frac{\partial f_i}{\partial t} + \mathbf{v} \cdot \nabla_{\mathbf{r}} f_i + \mathbf{E}_i \cdot \nabla_{\mathbf{v}} f_i = (f_i)_c \quad (\text{II-5})$$

where \mathbf{F}_i is the total specific force (force/mass) on the ions containing the electric and Lorentz forces. The term on the right expresses rate of change in the distribution function as a result of collisions between ions and species “s”, and may in principle contain both elastic and inelastic contributions. By taking the product of Eq. (II-5) with the ion momentum $m_i \mathbf{v}_i$ and integrating over velocity space one obtains the conservation law for momentum transport:

$$\frac{\partial}{\partial t} (nm \langle \mathbf{v} \rangle)_i + \nabla_r \cdot (nm \langle \mathbf{v} \mathbf{v} \rangle)_i - n_i m_i \langle (\mathbf{F} \cdot \nabla_v) \mathbf{v} \rangle_i = \int m_i \mathbf{v} (\dot{f}_i)_c d\mathbf{v} \quad (\text{II-6})$$

Recall the definitions of the relevant velocities: \mathbf{v} is the particle velocity (with respect to the laboratory frame of reference), $\mathbf{u} = \langle \mathbf{v} \rangle = n^{-1} \int \mathbf{v} f d\mathbf{v}$ is the mean particle velocity and $\mathbf{c} = \mathbf{v} - \mathbf{u}$ is the particle thermal velocity. Hereinafter, the subscript from the spatial operator ∇_r shall be excluded. Accordingly, the various terms in Eq. (II-6) are identified as follows:

$$\begin{aligned} \frac{\partial}{\partial t} (nm \langle \mathbf{v} \rangle)_i &= \frac{\partial}{\partial t} (nm \mathbf{u})_i \\ \nabla \cdot (nm \langle \mathbf{v} \mathbf{v} \rangle)_i &= \nabla \cdot [nm \langle (\mathbf{c} + \mathbf{u})(\mathbf{c} + \mathbf{u}) \rangle]_i = \nabla \cdot (nm \langle \mathbf{c} \mathbf{c} \rangle + nm \mathbf{u} \mathbf{u})_i \\ n_i m_i \langle (\mathbf{F} \cdot \nabla_v) \mathbf{v} \rangle_i &= n_i q_i \langle \mathbf{E}' \rangle \equiv n_i q_i \mathbf{E} \\ \int m_i \mathbf{v} (\dot{f}_i)_c d\mathbf{v} &\equiv \mathbf{R}_i \end{aligned} \quad (\text{II-7})$$

and note the appearance of the pressure tensor $\mathbf{p} = nm \langle \mathbf{c} \mathbf{c} \rangle$, which is many times expressed as the sum of two terms that separate the diagonal (\mathbf{pI}) from the off-diagonal ($\mathbf{\Pi}$) contributions to the tensor. The drag force density \mathbf{R}_i is defined in terms of the collision term on the right in Eq. (II-6). As in the case of the pressure tensor, \mathbf{R}_i may also be broken up into two parts to distinguish the momentum exchange between species by elastic collisions from that by inelastic collisions:

$$\mathbf{R}_i = \int m_i \mathbf{v} (\dot{f}_i)_c d\mathbf{v} \Big|_{\text{elastic}} + \int m_i \mathbf{v} (\dot{f}_i)_c d\mathbf{v} \Big|_{\text{inelastic}} \quad (\text{II-8})$$

Because the dynamics of the direct and inverse elastic collisions are the same, the term for collisions with species “s” may be approximated in terms of a mean collision rate ν between ions and other species “s”

$$\int m_i \mathbf{v} (\dot{f}_i)_c d\mathbf{v} \Big|_{\text{elastic}} \approx - \sum_{s \neq i} n_s m_s \nu_{is} (\mathbf{u}_i - \mathbf{u}_s) \quad (\text{II-9})$$

The momentum conservation law for ions may therefore be expressed in conservative form as follows:

$$\frac{\partial}{\partial t} (nm \mathbf{u})_i + \nabla \cdot (nm \mathbf{u} \mathbf{u})_i = q_i n_i \mathbf{E} - \nabla \cdot \mathbf{p}_i + \mathbf{R}_i \quad (\text{II-10})$$

where we have neglected the viscous terms and assumed that $\mathbf{p}_i = p_i \mathbf{I}$ (with \mathbf{I} being the unit or delta tensor). Equation (II-10) may be combined with the ion continuity

$$\begin{aligned} \frac{\partial (nm)_i}{\partial t} + \nabla \cdot (nm \langle \mathbf{v} \rangle)_i &= \int m_i (\dot{f}_i)_c d\mathbf{v} \\ &\equiv m_i \dot{n} \end{aligned} \quad (\text{II-11})$$

to yield the momentum equation in non-conservative form

$$\begin{aligned}
n_i m_i \left[\frac{\partial \mathbf{u}_i}{\partial t} + (\mathbf{u}_i \cdot \nabla) \mathbf{u}_i \right] &= q_i n_i \mathbf{E} - \nabla \cdot \mathbf{p}_i + \mathbf{R}_i - \mathbf{u}_i m_i \dot{n} \\
n_i m_i \frac{D \mathbf{u}_i}{Dt} &\approx q_i n_i \mathbf{E} - \sum_{s \neq i} n_s m_s v_{is} (\mathbf{u}_i - \mathbf{u}_s) - \nabla \cdot \mathbf{p}_i + \mathbf{S}_i
\end{aligned} \tag{II-12}$$

where \mathbf{S}_i includes all the inelastic contributions to the transport of ion momentum,

$$\mathbf{S}_i \equiv \int m_i \mathbf{v} (f_i)_{\dot{c}} d\mathbf{v} - m_i \mathbf{u}_i \dot{n} \tag{II-13}$$

It is noted that there are two terms in \mathbf{S}_i and they are mathematically distinct. The first appears as a direct consequence of taking the first moment of Eq. (II-5) to obtain the conservative form of the momentum equation (II-10). The second term appears because Eqs (II-10) and (II-11) were combined to obtain the non-conservative form of the momentum equation (II-12). For a quasi-neutral plasma with only singly-charged ions and no recombination, \mathbf{S}_i takes the simple form

$$\mathbf{S}_i = m_i \mathbf{u}_n \dot{n} - m_i \mathbf{u}_i \dot{n} = -m_i n_e v_{en}^I (\mathbf{u}_i - \mathbf{u}_n) \tag{II-14}$$

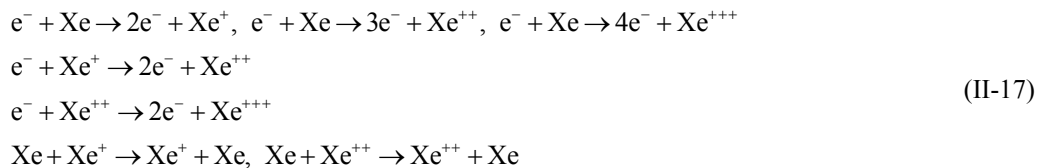
and, assuming only charge-exchange collisions for the elastic contributions in Eq.(II-9), Eq. (II-12) is simplified as follows:

$$n_i m_i \frac{D \mathbf{u}_i}{Dt} = q_i n_i \mathbf{E} - \nabla p_i - n_i m_i (v_{in} + v_{en}^I) (\mathbf{u}_i - \mathbf{u}_n) \tag{II-15}$$

to yield the ion velocity field. Multiply-charged ions may be accounted for by following the same formulations outlined above while including the relevant ionization collision frequencies for the higher charge states. The last term on the right of Eq. (II-15) may in fact be expressed more generally in terms of an ion rate that includes both charge-exchange and electron impact-ionization collisions as follows:

$$-m \sum_{i' \rightarrow i} \dot{n}_{i' \rightarrow i} (\mathbf{u}_i - \mathbf{u}_{i'}) \tag{II-16}$$

with $i' \rightarrow i$ denoting the direction of the reaction. For example, for collisions that generate singly-charged ions from neutrals, $\text{Xe} \rightarrow \text{Xe}^+$, then $i'=0$ and $i=1$ and so forth and so on. In the present model we account for the following reactions listed in Eq. (II-17) with all collision cross-sections specified based on available data. However, the drag between multiply-charged species $\sim n_i^Z m_i v_{ii}^Z (\mathbf{u}_i^Z - \mathbf{u}_i^{Z+1})$ has not yet been included.



For the results presented in this paper a constant temperature of 500 °C has been assumed for the ions. Although no sensitivity calculations have been performed yet to assess the impact of the assumption on the solution, it is not expected to have a significant effect since the ion temperature affects only the ion pressure and the ion-neutral collision frequencies. On-average the latter has a square-root dependence on the temperature and the ion-pressure gradient force is negligible compared to the other forces; this will be further quantified in an ensuing section. Also, in the case of heavy species with different masses, m in expression (II-16) would be proportional to the reduced mass, $m_i m_j / (m_i + m_j)$, but since here only xenon ions and atoms are present m denotes the mass of the heavy species.

The system of conservation laws for the ions is closed with conditions specified at all boundaries in Figure 1. At the anode and dielectric-wall boundaries the Bohm condition is prescribed for all ion species. At the plume boundaries the ions are allowed to flow out of the system freely (gradients of the two velocity components are set to

zero). Reflection boundary conditions are set at the axis of symmetry. Presently no ion flux is specified to flow out of the cathode boundary.

2) Numerical approach

Equation (II-15) is solved using a first-order upwind scheme for the velocity field at the vertices, \mathbf{u}_{ver} . Since the computational region is comprised of quadrilateral computational cells of arbitrary shape the scheme accounts for the surrounding eight vertices (open circles) to determine the upwind direction (Figure 3-left). Because all the conservation laws in Hall 2De are discretized using finite-volume differencing, scalars (such as number density n_{cel}) are computed at the cell centers and vectors (such as forces \mathbf{F}_{edg} and fluxes) are computed at the cell edges. The ion momentum equation is the only conservation law solved in non-conservative fashion so it requires that both vectors and scalars be known at vertices. The algorithm employs bilinear interpolation at each vertex for edge-centered (Figure 3-middle) and cell-centered quantities (Figure 3-right) using the quadrilateral defined by the dashed lines in Figure 3. Equations (II-11) and (II-15) are marched explicitly from time t to yield new values for the ion density and velocity field at $t+\Delta t$.

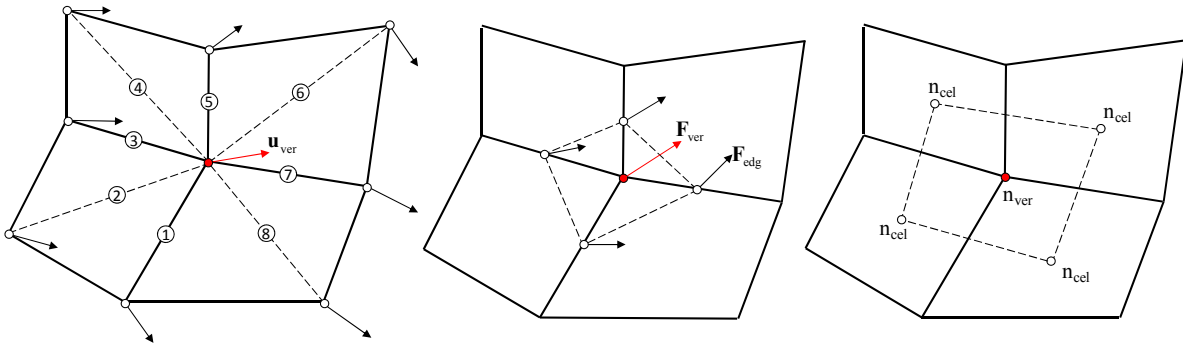


Figure 3. Left: The ion momentum equation is solved in non-conservative form for the velocity field at the vertices using a 1st-order upwind scheme that takes into account the contributions from a maximum of eight surrounding vertices. Middle: Bilinear interpolation is used to define forces at vertices using their primitive values at the cell edges. Right: Bilinear interpolation is used to define scalar quantities at vertices using their primitive values at the cell centers.

A. Electrons

1) Physics model

The electron momentum equation in the absence of the viscous terms and assuming $\mathbf{p}_e = p_e \mathbf{I}$ is given in vector form by:

$$n_e m_e \frac{D\mathbf{u}_e}{Dt} = -en_e (\mathbf{E} + \mathbf{u}_e \times \mathbf{B}) - \nabla p_e + \mathbf{R}_e \quad (\text{II-18})$$

As in the case for ions, the friction force \mathbf{R}_e/n_e for electrons is related to the integral of the collision term in the electron distribution function and the electron momentum. For the case of a near (or “quasi”)-Maxwellian distribution function in an anisotropic, classical plasma (i.e. with no random fluctuations in the fields) \mathbf{R}_e may be approximated as follows, assuming $\mathbf{u}_e \gg \mathbf{u}_n$:

$$\mathbf{R}_e \approx -n_e m_e \left[\sum_i v_{ei} (\mathbf{u}_e - \mathbf{u}_i) + v_{en} \mathbf{u}_e \right] = e^{-1} m_e (\bar{v}_{ei} + v_{en}) \mathbf{j}_e + (eZ^*)^{-1} m_e \bar{v}_{ei} \sum_i Z \mathbf{j}_i \quad (\text{II-19})$$

with the electron and ion current densities defined as $\mathbf{j}_e = -en_e \mathbf{u}_e$ and $\mathbf{j}_i = q_i n_i \mathbf{u}_i = eZ n_i \mathbf{u}_i$ respectively, and the total e-i collision rate given by

$$\bar{v}_{ei} = \frac{n_e Z^* e^4 \ln \Lambda}{3(2\pi)^{3/2} \epsilon_0^2 \sqrt{m_e} (k_B T_e)^{3/2}} \quad Z^* \equiv n_e^{-1} \sum_i n_i Z_i^2 \quad (\text{II-20})$$

Unless otherwise noted, all references to “e-i collision rate” in the remainder of this paper shall imply the definition in Eq. (II-20). If the electron inertia can be neglected then one obtains the vector form of Ohm’s law

$$\mathbf{E} = \eta_0 \mathbf{j}_e + \eta_0 \Omega_0 \mathbf{j}_e \times \hat{\boldsymbol{\beta}} - \frac{\nabla p_e}{en_e} + \eta_{ei} \bar{\mathbf{j}}_i \quad (\text{II-21})$$

where

$$\eta_0 = \frac{m_e (\bar{v}_{ei} + v_{en})}{e^2 n_e} \quad \eta_{ei} = \frac{m_e \bar{v}_{ei}}{e^2 n_e} \quad \hat{\boldsymbol{\beta}} = \mathbf{B}/B \quad \Omega_0 = \frac{|B|}{en_e \eta_0} \quad \bar{\mathbf{j}}_i = \frac{1}{Z^*} \sum_i Z_i \mathbf{j}_i \quad (\text{II-22})$$

In the frame of reference of the magnetic induction field with “//” and “ \perp ” denoting parallel and perpendicular components respectively, the components of Eq. (II-21) may be written as

$$E_{//} = \eta_0 j_{e//} - \frac{\nabla_{//} p_e}{en_e} + \eta_{ei} \bar{j}_{i//} \quad E_{\perp} = \eta_0 (1 + \Omega_0^2) j_{e\perp} - \frac{\nabla_{\perp} p_e}{en_e} + \eta_{ei} \bar{j}_{i\perp} \quad (\text{II-23})$$

It is noted that in the absence of the ion velocity in the electron drag force density (Eq. (II-19)), Eqs (II-23) take a form that is suitable for problems involving electron diffusion in weakly-ionized plasmas, and has traditionally been used in Hall thruster models such as HPHall⁷:

$$j_{e//} = en_e \mu_0 \left(E_{//} + \frac{\nabla_{//} p_e}{en_e} \right) \quad j_{e\perp} = \frac{en_e \mu_0}{1 + \Omega_0^2} \left(E_{\perp} + \frac{\nabla_{\perp} p_e}{en_e} \right) \quad (\text{II-24})$$

and uses the electron mobility μ_0 instead of the resistivity (note $\mu_0 = 1/en_e \eta_0$). Equations (II-24) imply the approximation $\mathbf{u}_e \gg \mathbf{u}_i$ and $\mathbf{u}_e \gg \mathbf{u}_n$ and thus $\mathbf{R}_e \approx -n_e m_e v_0 \mathbf{u}_e$ with the total collision rate “ v_0 ” representing the contributions from classical collisions of electrons with all other species. It has also been suggested that the diffusion of electrons is enhanced in a non-classical manner, e.g. by plasma turbulence, and attempts to capture this enhancement in HPHall numerical simulations have been made through the use of an effective collision rate based on Bohm’s $1/B$ scaling for the cross-field mobility.⁹ That is, $\mathbf{R}_e \approx -n_e m_e (v_0 + v_B) \mathbf{u}_e$ where,

$$v_B = \frac{\alpha}{16} \omega_{ce} \quad (\text{II-25})$$

with α being a constant. During their azimuthal drift electrons may also collide with walls and this has been proposed (originally by Morozov¹⁹) to be one more process that effects the transport of electrons in the acceleration channel. In numerical simulations of Hall thrusters this additional transport mechanism has been accounted for through the addition of another effective collision rate v_{ew} . Accounting for all transport mechanisms an effective electrical resistivity and Hall parameter may be defined as

$$\eta \equiv \frac{m_e (\bar{v}_{ei} + v_{en} + v_{ew} + v_B)}{e^2 n_e} \quad \Omega_e \equiv \frac{|B|}{en_e \eta} \quad (\text{II-26})$$

Unless otherwise noted, all references to “Hall parameter” in the remainder of this paper shall imply the definition in Eq. (II-27). In Section III a series of numerical simulations will be presented that compare results obtained by Hall 2De with those obtained recently by HPHall for two Hall thrusters, namely the BPT-4000 and the 6 kW Hall thruster. In these simulations the HPHall solutions incorporate a spatially varying α that is guided by plasma measurements and by the observed operational characteristics of the thrusters (such as discharge current and thrust).

The presence of turbulence, its real effect on electron transport and the question of whether it can be quantified using Bohm's formula has been an ongoing area of research. As a consequence, the variation of α from one thruster simulation to another is not based on first principles, which poses the biggest challenge in the development of a predictive theoretical model of Hall thrusters.

The overall system of conservation laws is augmented with an equation for the conservation of current

$$\nabla \cdot (\mathbf{j}_e + \mathbf{j}_i) = 0 \quad (\text{II-27})$$

and the equation for the electron temperature (expressed in eV)

$$\frac{3}{2} n_e \frac{\partial T_e}{\partial t} = \mathbf{E} \cdot \mathbf{j}_e + \nabla \cdot \left(\frac{5}{2} T_e \mathbf{j}_e + \boldsymbol{\kappa}_e \cdot \nabla T_e \right) - \frac{3}{2} T_e \nabla \cdot \mathbf{j}_e - \sum_s \dot{n}_s e \left(\epsilon_s + \frac{3}{2} T_e \right) + Q_e^T \quad (\text{II-28})$$

The last term on the right represents the energy exchange per unit time between electrons and the heavy species due to deviations from thermal equilibrium and is proportional to $n_e(m_e/m)v_{ei}(T_e-T_i)$ for ions and $n_e(m_e/m)v_{en}(T_e-T_n)$ for neutrals. In Hall thrusters it is usually a small contribution to the total electron energy content.

The equations for the electrons are closed with boundary conditions at all surfaces in Figure 1. As it will be shown in the next subsection, Eq. (II-27) is in fact combined with Eq. (II-23) to yield the plasma potential, and requires boundary conditions either for the plasma potential, its gradient or for the current density. For all dielectric-wall boundaries a zero-current condition is imposed, $\mathbf{j}_e = \mathbf{j}_i$. At the anode a Dirichlet condition specifies directly the voltage at its discharge value. For both simulation cases that are presented in this paper this value is 300 V. A Dirichlet condition is also imposed at the cathode with a value of 0 V. For the electron energy the convective heat loss follows the formulations of Hobbs and Wesson (H&W)²⁹ using a fit³⁰ for the H&W solution of the sheath potential as a function of the secondary electron yield (SEE). The Maxwellian-averaged SEE is also specified using a fit to data for the dielectric material used in each thruster. A Dirichlet condition for the electron temperature is also currently imposed at the anode.

2) Numerical approach

The large disparity (>2 orders of magnitude in regions with high values of the magnetic field) that exists in the electron transport equations in the perpendicular versus the parallel direction requires special treatment. One approach is to solve the equations for electrons only in the perpendicular direction; this quasi-1D approach followed by HPHall and other similar models of Hall thrusters. This evades the numerical difficulties associated with the resolution of transport in both directions and is an excellent approximation for most of the acceleration channel and near-plume regions. To extend the solution to regions in the far plume and/or to resolve regions of the magnetic field with complex topology requires a 2-D solution of the electron transport equations. The approach followed here is to solve the equations in the frame of reference of the magnetic field, in two dimensions ($\hat{\boldsymbol{\beta}} = \beta_r \hat{\mathbf{r}} + \beta_z \hat{\mathbf{z}}$). To diminish excessive numerical diffusion all equations are discretized in a computational mesh that is aligned with the magnetic field lines. In this section this general approach is outlined using Eq. (II-27) as the example equation.

The plasma potential in Hall 2De is solved by combining current conservation and Ohm's law into one equation. Then for a single quadrilateral computational cell with volume ΔV the divergence theorem allows for the following discretization:

$$\begin{aligned} \nabla \cdot \mathbf{j}^{t+\Delta t} \Delta V &= \sum_{\text{edg}=1}^4 (\mathbf{j}^{t+\Delta t} \cdot \hat{\mathbf{n}} \Delta A)_{\text{edg}} \\ &= \sum_{\text{edg}=1}^4 \left\{ \left[(\mathbf{j}^{t+\Delta t} \cdot \hat{\boldsymbol{\beta}}) \hat{\boldsymbol{\beta}} - \hat{\boldsymbol{\beta}} \times (\hat{\boldsymbol{\beta}} \times \mathbf{j})^{t+\Delta t} \right] \cdot \hat{\mathbf{n}} \Delta A \right\}_{\text{edg}} \end{aligned} \quad (\text{II-29})$$

The dot product in Eq. (II-29) for each edge may be expanded as

$$\left[(\mathbf{j}^{t+\Delta t} \cdot \hat{\boldsymbol{\beta}}) \hat{\boldsymbol{\beta}} - \hat{\boldsymbol{\beta}} \times (\hat{\boldsymbol{\beta}} \times \mathbf{j})^{t+\Delta t} \right] \cdot \hat{\mathbf{n}} \approx \eta^{-1} (\mathbf{E}^{t+\Delta t} + \boldsymbol{\varepsilon}^t) \cdot \hat{\mathbf{n}}^t \quad (\text{II-30})$$

where

$$\begin{aligned}\bar{\mathbf{n}} &\equiv \bar{\mathbf{n}}_r + \bar{\mathbf{n}}_z \\ \bar{\mathbf{n}}_r &= \beta_r (\beta_r \hat{\mathbf{r}} + \beta_z \hat{\mathbf{z}}) \cdot \hat{\mathbf{n}} + \frac{\beta_z}{1 + \Omega_e^2} (\beta_z \hat{\mathbf{r}} - \beta_r \hat{\mathbf{z}}) \cdot \hat{\mathbf{n}} \\ \bar{\mathbf{n}}_z &= \beta_z (\beta_r \hat{\mathbf{r}} + \beta_z \hat{\mathbf{z}}) \cdot \hat{\mathbf{n}} - \frac{\beta_r}{1 + \Omega_e^2} (\beta_z \hat{\mathbf{r}} - \beta_r \hat{\mathbf{z}}) \cdot \hat{\mathbf{n}}\end{aligned}\quad (\text{II-31})$$

and $\mathbf{E} = -\nabla\phi$. The remaining terms in Eq. (II-23) involving the electron pressure and the ion current terms are included in $\boldsymbol{\varepsilon}$. Equation (II-29) is solved implicitly for the plasma potential. It is noted that a simplification occurs in Eqs (II-31) when the computational mesh is aligned with the magnetic field, as illustrated in Figure 4. Numerical diffusion due to the disparity between the terms with and without Ω_e is reduced by assuming that cell edges are exactly either parallel or perpendicular to the magnetic field lines, and the accuracy of the solution is then dependent upon the extent of the spatial deviations of the mesh from the true lines of constant potential and stream functions χ and ψ . Here, χ and ψ are the commonly-used set of conjugate harmonic functions satisfying the Cauchy-Riemann conditions for the radial and axial components of the magnetic (vector) field.

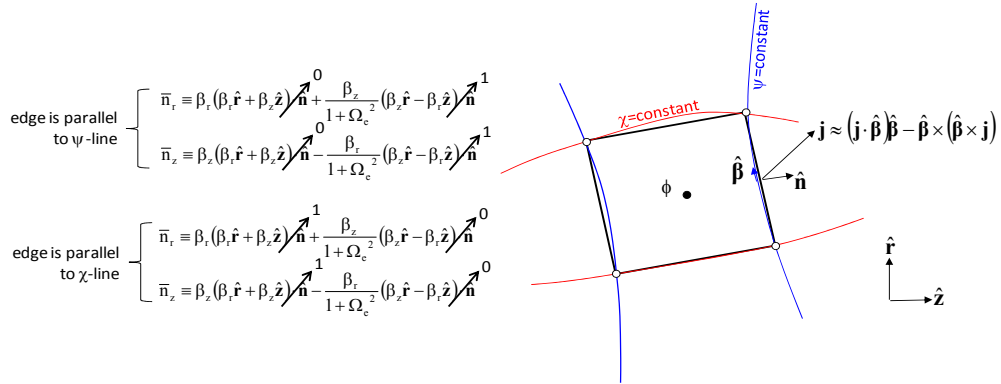


Figure 4. Each edge of a computational cell in Hall 2De is closely aligned with either a line of constant potential function (χ) or a line of constant stream function (ψ).

The computational mesh is generated first by superimposing lines of constant χ and ψ onto the computational region using commercially available graphics software (Figure 5-left). The computational region boundaries are specified by line segments that connect points used to specify the geometry of the region. Then the spatial locations of points along each line, generated by integration in space along each streamline, are extracted. Each pair of adjacent points along a χ -line (or a ψ -line) defines a line segment. A mesh algorithm then searches for the intersections between all line segments over all χ -lines, ψ -lines and boundary lines. Each intersection defines a vertex location and these vertices are then used to generate the finite element mesh shown in Figure 5-right.

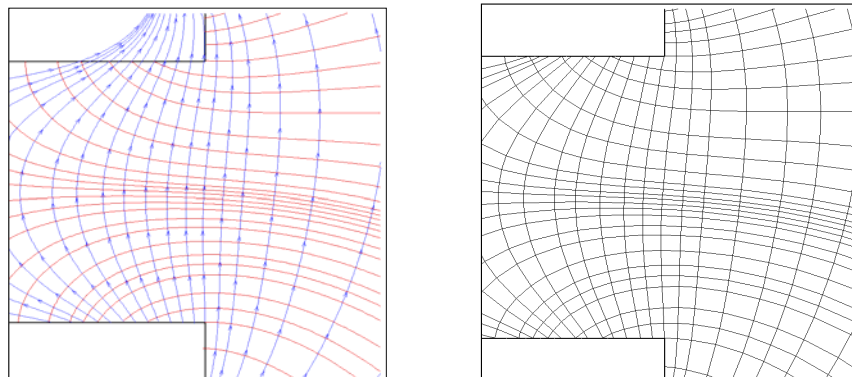


Figure 5. Left: A set of lines of constant stream function (ψ) in blue (streamlines of the magnetic field) overlaid by lines of constant potential function (χ) in red, in the vicinity of the acceleration channel in the 6 kW Hall thruster. Right: corresponding finite-element computational mesh.

The equation for the electron temperature is solved in a semi-implicit fashion. The thermal conduction term is implicit whereas all other terms are evaluated at the previous time-step as expressed by Eq. (II-32).

$$\frac{3}{2} n_e^t \frac{T_e^{t+\Delta t} - T_e^t}{\Delta t} - \nabla \cdot (\kappa_e^t \cdot \nabla T_e^{t+\Delta t}) \approx \left[\mathbf{E} \cdot \mathbf{j}_e + \nabla \cdot \left(\frac{5}{2} T_e \mathbf{j}_e \right) - \frac{3}{2} T_e \nabla \cdot \mathbf{j}_e - \sum_s \dot{n}_s e \left(\varepsilon_s + \frac{3}{2} T_e \right) + Q_e^T \right]^t \quad (\text{II-32})$$

III. Numerical Simulations

A. Benchmark simulations of the BPT-4000

As a first series of Hall 2De algorithm tests we performed comparisons with existing numerical simulation results¹² obtained by HPHall for the BPT-4000 operating at 4.5 kW. The operational characteristics of this thruster as used in the numerical simulations are outlined in Table 1. The simulations employed the same spatial variations of the Bohm collision rate factor α in the acceleration channel and near-plume regions as in the HPHall simulations. It is noted that in those simulations the factor was significantly lower inside the acceleration channel ($\alpha=0.035$) compared to the plume region ($\alpha=1.0$). Moreover, beyond the effective HPHall computational region, defined by a near-anode magnetic-field streamline and a near-cathode streamline (as illustrated in Figure 6) both the Bohm collision rate and the Hall parameter are specified as zero. For this first series of algorithm tests the same spatial variations for v_B and Ω_e are specified in Hall 2De as in HPHall but with a slightly more gradual reduction to zero (using a Gaussian function) downstream of the cathode field line. The one-on-one comparisons along a line that crosses the middle of the acceleration channel are shown in Figure 7 (top). The benchmark simulations have also used the same model for the wall collision rate $v_{e\text{-wall}}$.

The axial comparisons in Figure 7 and the 2-D contour plots in Figure 8 show similar solutions but with some marked differences. The overall heating of electrons appears to be in close agreement between the two solutions, which is expected since the peak electron temperature and the spatial variation near this maximum is driven mainly by resistive heating that is dominated by the Bohm collision rate. By comparison to the other collision frequencies v_B is at least one order of magnitude higher at the exit and near-plume regions where the maximum in the temperature is computed. Near the anode the electron temperature in Hall 2De is determined largely by the anode Dirichlet boundary condition (currently specified as 1 eV) and the surrounding dielectric-wall conditions, which prescribe the same H&W solution²⁹ as in HPHall for the convective heat loss of electrons in the sheath.

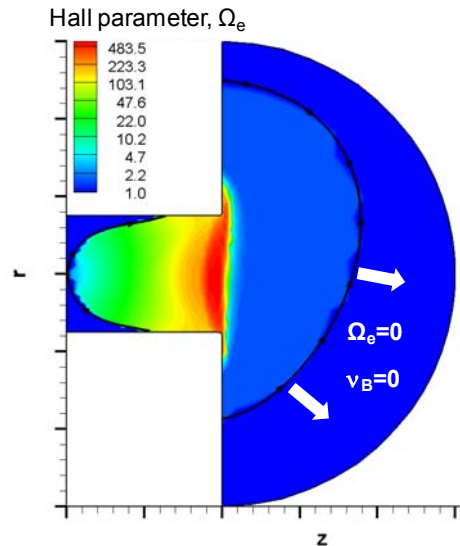


Figure 6. Contours of the Hall parameter as computed by HPHall in the 6 kW Hall thruster simulations.¹³ Near-anode and near-cathode streamlines define the effective HPHall computational domain beyond which Ω_e and v_B are set to zero. The same approach is followed in the BPT-4000 simulations.¹²

Table 1. Operational characteristics used in the numerical simulations of the BPT-4000 at 4.5 kW.

Thruster parameter	Value
Discharge (or anode) current (A)	15
Discharge voltage (V)	300
Anode mass flow rate (mg/s)	15.5
Cathode mass flow rate (mg/s)	1.55

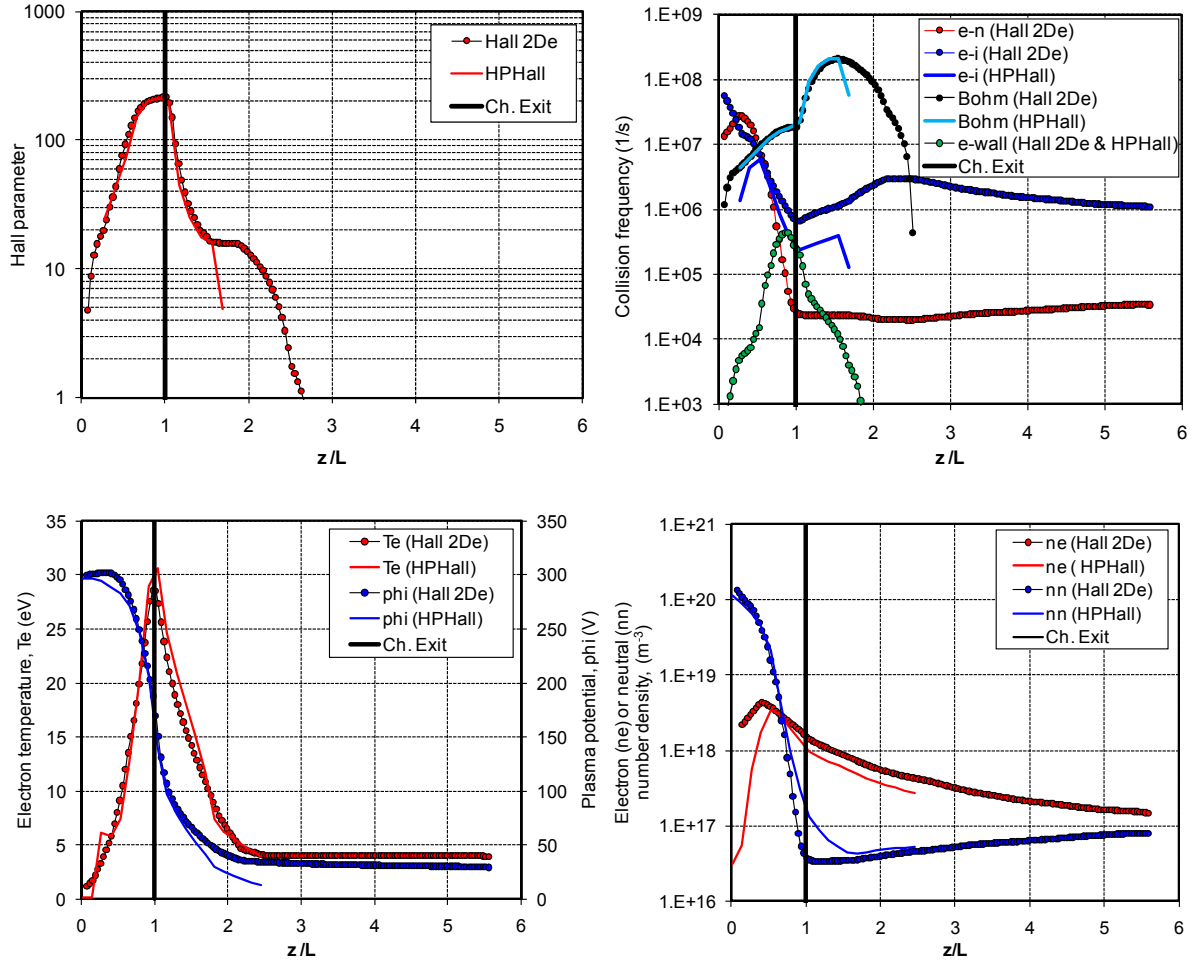


Figure 7. Axial slice plots from the benchmark numerical simulations of the BPT-4000. The plots compare the solution¹² obtained by HPHall with that obtained by Hall 2De at the middle of the acceleration channel. The channel length is denoted by L . In these benchmark simulations the Hall 2De simulations enforce a reduction of the Bohm collision rate and of the Hall parameter beyond $z/L \sim 1.5$ to emulate the approach followed in the HPHall simulations.

A notable distinction between the solutions for the electron number density and plasma potential is evident in the anode region. This is illustrated in Figure 7 (bottom), Figure 8 (top), and is more evident in the axial profiles of Figure 9 (left). Hall 2De computes a higher plasma density in this region with values for $z/L < 0.2$ exceeding one order of magnitude those obtained by HPHall. A comparison of the terms in Eq. (III-1) show that the anode region is dominated by ion diffusion since this is where the electric-field force is negligible. It is noted that as part of the inherent assumptions associated with the PIC simulation of ions the ion drag terms (numbered as “IV” in Eq. (III-1)) are not accounted for in HPHall. The ion pressure is also not included in HPHall and the Hall 2De simulations confirm this to be a good assumption for the assumed ion temperature. The comparison of all the ion momentum terms is shown in Figure 9, right. The effect of mesh resolution on the solution has not yet been quantified but, if of any significance, this is expected to influence the solution only in the very-near anode regions where the mesh is coarsest.

$$\frac{\partial \mathbf{u}_i}{\partial t} \approx \underbrace{\frac{q_i}{m_i} \mathbf{E}}_{(I)} + \underbrace{(-\mathbf{u}_i \cdot \nabla) \mathbf{u}_i}_{(II)} + \underbrace{\frac{-\nabla p_i}{n_i m_i}}_{(III)} + \underbrace{(\mathbf{v}_{in} + \mathbf{v}_{en}^I)}_{(IV)} (\mathbf{u}_n - \mathbf{u}_i) \quad (III-1)$$

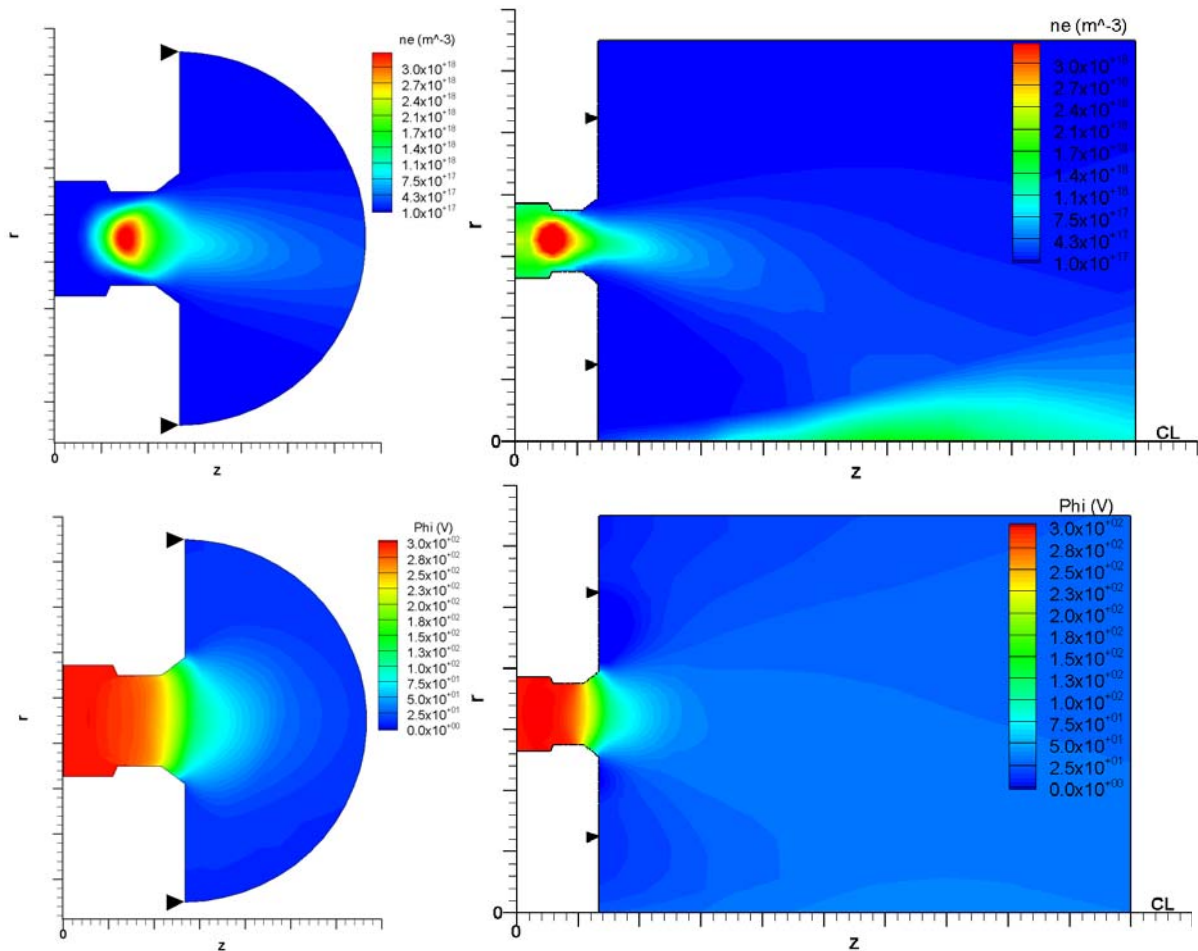


Figure 8. Contour plots from the numerical simulations of the BPT-4000. The plots compare the 2-D solution¹² obtained by HPHall (left) with that obtained by Hall 2De (right). For these benchmark simulations the two computer codes use approximately the same model for the spatial variation of the Bohm collision rate. The arrows point to the maximum radial extent of the HPHall computational region. Top: electron number density. Bottom: plasma potential.

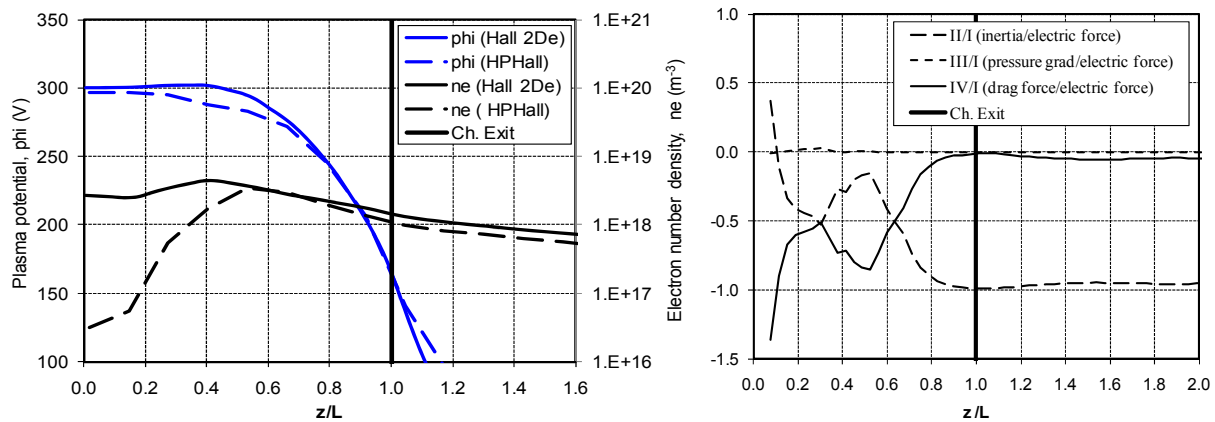


Figure 9. Comparison of terms in the ion momentum conservation law for singly charged ions (Eq. (III-1)) along the mid-channel line of the BPT-4000 for the steady-state benchmark simulation case. The profiles on the right identify the anode or “ion-diffusion” region ($z/L < -0.3$), the ionization region ($0.3 < z/L < 0.6$) and the ion-acceleration region ($z/L > 0.6$).

A related effect is associated with the variation of the electric field in this region where measurements³¹ have suggested little to no variation of the plasma potential (i.e. $E_z \approx 0$). Similar comparisons as those performed for the ion momentum may be carried out for the dominant terms in Ohm's law, namely the resistive term and the electron pressure. These suggest that the increased plasma density reduces significantly the importance of these terms in this region such that any differences between them (the numerator in Eq. (III-2)), that would otherwise generate a finite electric field, are reduced. The numerator in Eq. (III-2) is also reduced since the total classical collision rate is higher (first term) and the density gradient is lower (second term) compared to the HPHall solution.

$$E_{\perp} \approx \eta_0 \left(1 + \Omega_e^2\right) j_{e,\perp} - \frac{\nabla_{\perp} p_e}{en_e} \sim \frac{j_{e,\perp} B^2 / m_e (v_{ei} + v_{en}) - T_e \nabla_{\perp} n_e}{n_e} \quad (\text{III-2})$$

The e-i collision rate is found to be higher in the near-plume regions as well, in part due to the higher plasma density there but largely as a result of accounting for the multiply-charged ions in Eq. (II-20) (through Z^*); more notable however in the Hall 2De results is its continued rise downstream of the HPHall computational region. This rise is largely due to the colder electron temperature since the rate is proportional to $T_e^{-3/2}$. The capacity to resolve this rise due to Hall 2De's extended computational region prompted a series of preliminary simulations to better understand the response of the plasma, specifically that of the electron-ion (e-i) collision rate, since it dominates over both the electron-neutral (e-n) and the electron-wall frequencies beyond the ionization region. Figure 10-left shows the computed e-i collision rate for three different values of the maximum Bohm factor, $\alpha=1.0, 0.2$ and 0.05 . It should be clarified that we use "maximum" here because, as also noted earlier, α is varied in the physical domain: for the BPT-4000 benchmark simulations in Figure 7 ($\alpha \equiv \alpha_c$ in Ref. 12)=0.035 inside the channel, $\alpha \equiv \alpha_p$ in Ref. 12)=1.0 in the near-plume and for $z/L > 1.5$ α_p is reduced to zero. So, when we decrease the Bohm factor in this paper to, say, $\alpha=0.2$ we imply a global reduction of the Bohm collision rate, that is $v_B = (0.035 \times 0.2) \omega_{ce} / 16 = 0.007$ inside the channel and $v_B = (1.0 \times 0.2) \omega_{ce} / 16 = 0.2 \omega_{ce} / 16$ in the near-plume.

The results in Figure 10-left show an increasing e-i collision rate with decreasing α mainly because of the reduced electron temperature in the near-plume. The plasma density is also found to increase along the mid-channel line. The computed profiles for the electron temperature are shown in Figure 11. The anode current (15 A) is obtained for a maximum $\alpha \approx 0.2$, an 80% lower value than that used in the Hall 2De-HPHall benchmark simulations. For this spatial variation and value of maximum α the ion (beam) current is found to $I_b = (I^+) + (I^{++}) + (I^{+++}) = 9.7 + 4.5 + 0.3 = 14.5$ A. Also, the solution for the anode and beam currents in Figure 10-right exhibits a periodic character but one that is under-damped; all current oscillations die out within a few periods. The damping of the oscillations occurs faster (within a period) for $\alpha=1.0$ and produces ~ 3.5 A more anode current than the nominal value. The case of $\alpha=0.05$ produces current oscillations that do not die out albeit at 1.2 A lower time-averaged anode current. We postulate that the lack of dependence of the Bohm collision rate on any of the plasma parameters may be responsible for the damping of the oscillations at the high values of α . Low-frequency oscillations in the Hall 2De solution at low values of α are also obtained in the 6 kW Hall thruster simulations to be presented in the next subsection.

The increase of the e-i collision rate to values that are comparable or higher than the Bohm collision rate is of significance in part because, to the best of our knowledge, the transport of electrons from regions of the plume that extend beyond the HPHall physical domain have not yet been resolved. In view of the elevated values of the e-i collision rate in the far-plume, in the next section we attempt to lift the reduction of the Hall parameter and Bohm collision rate that was imposed as part of the benchmark simulations with the BPT-4000. In recognition of the sensitivity of the e-i collision rate on the electron temperature, we end this section with a calculation that assesses the influence of the far-plume boundary condition. Figure 12 compares the computed rate at the channel midline for two cases. The first case specifies $T_e = 1$ eV at the horizontal and vertical far-plume boundaries (see Figure 1) and the second case sets $T_e = 4$ eV at these boundaries. As expected, the near-plume and channel regions are not found to be significantly affected whereas the far-plume regions are largely driven by the boundary value. Recent plasma measurements in the far-plume regions indicate that the temperature several channel heights downstream of the exit is 4-5 eV.³² A value of 4 eV has been used for the BPT-4000 benchmark simulations shown in Figure 7 and Figure 8. The results in Figure 11 on the effects of α were obtained with $T_e = 1$ eV at the far-plume boundaries and the qualitative trends associated with e-i collision rate are found to be unaffected by this value. The ensuing simulations with the 6 kW Hall thruster use $T_e = 4$ eV at the boundaries based on plasma measurements.¹³

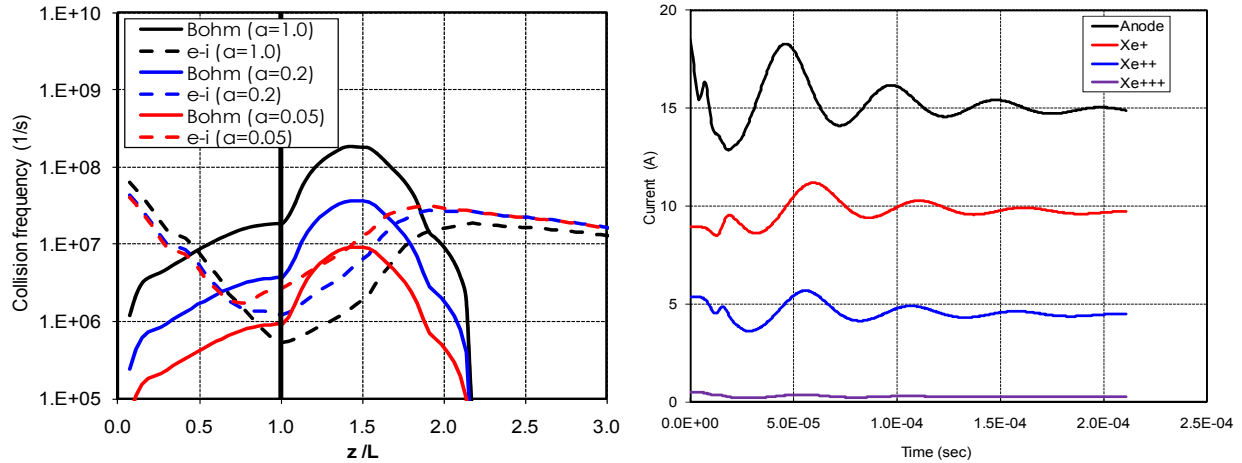


Figure 10. Left: The response of the classical e-i collision rate to reductions of the imposed Bohm collision rate (through the Bohm factor α) along a line at the middle of the acceleration channel. Right: The computed anode and beam currents as a function of time for $\alpha=0.2$.

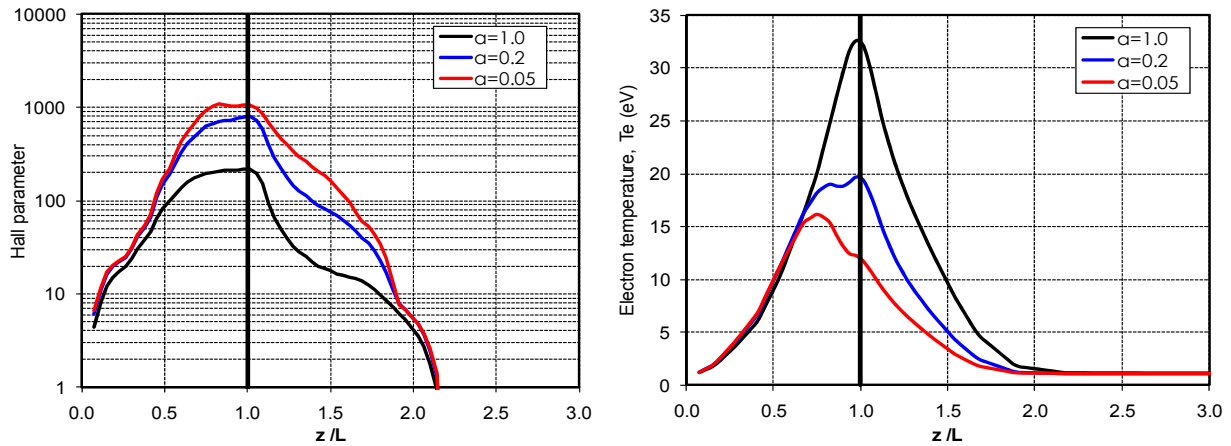


Figure 11. The response of the Hall parameter Ω_e (left) and the electron temperature (right) to reductions of the imposed Bohm collision rate (through the Bohm factor α) along a line at the middle of the acceleration channel.

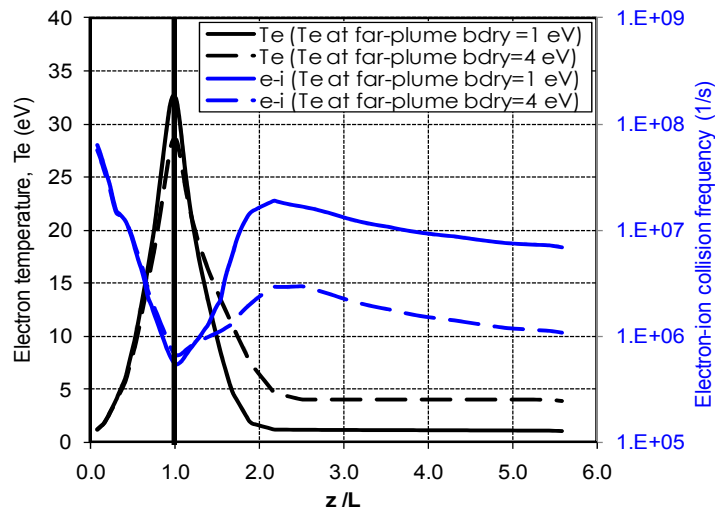


Figure 12. Sensitivity of the electron-ion collision rate on the far-plume boundary conditions for the electron temperature.

B. Extended simulations with the 6-kW laboratory Hall thruster

In this section we extend the studies of Section III.A on the effects of reduced Bohm collision rate to a 6 kW laboratory Hall thruster. This thruster has a simpler channel geometry compared to the BPT-4000, and has been operated and studied for fundamental research at several institutions.^{31,33,34,35} Also, several measurements have been obtained³¹ with the cathode placed at the axis of symmetry (e.g. see photo in Table 2). This cathode-thruster arrangement is of great interest in numerical simulations because it is 2-D axisymmetric. The operational characteristics for the simulations presented in this paper are outlined in Table 2. The magnetic field arrangement, physical domain and field-aligned computational mesh are shown in Figure 13.

Table 2. Operational characteristics used in the numerical simulations of the 6 kW laboratory Hall thruster.

Thruster parameter	Value
Discharge (or anode) current (A)	20
Discharge voltage (V)	300
Anode mass flow rate (mg/s)	20.98
Cathode mass flow rate (mg/s)	1.47

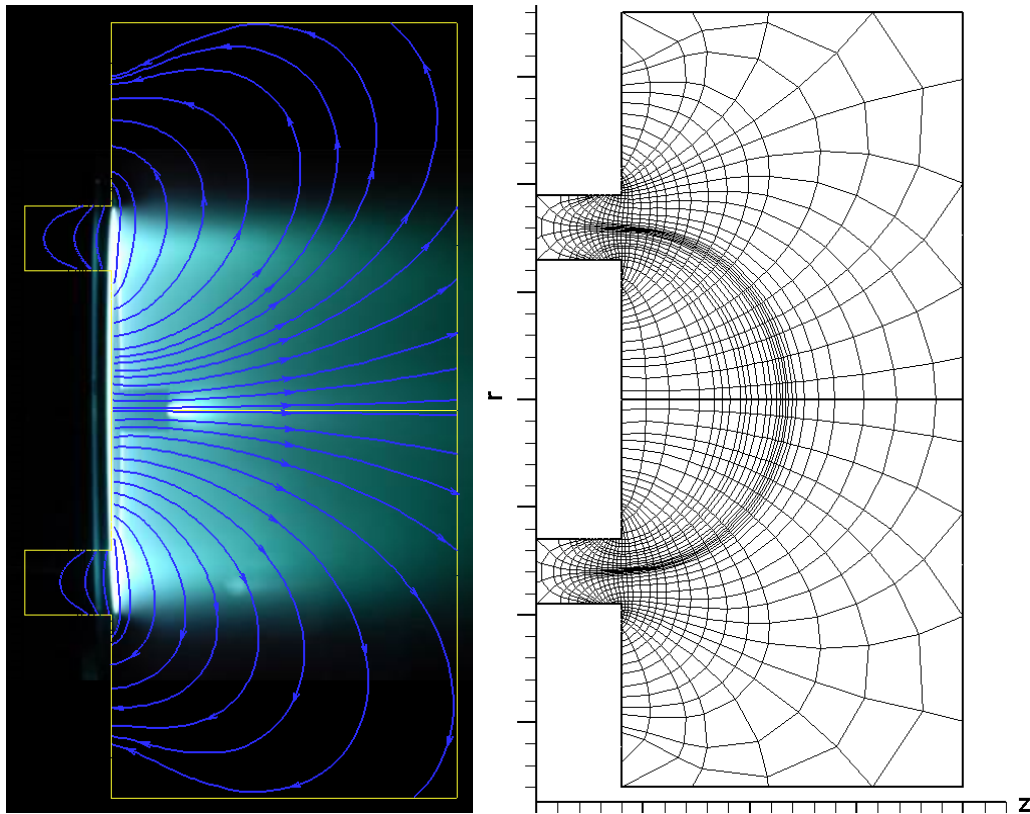


Figure 13. Physical domain, magnetic field and computational mesh for the numerical simulations of the 6 kW laboratory Hall thruster.

The solid curves in Figure 14 depict the Hall 2De solution with a reduction of the Bohm collision rate and Hall parameter in the far-plume similar to that implemented in the BPT-4000 simulations. It is found that the maximum value of α , with the prescribed spatial arrangement shown by the solid curve in Figure 14, that yields the observed anode current is 0.4. These set of simulation results have been obtained to allow for direct comparisons with ensuing simulations that lift the constraints on v_B and Ω_e . The computed anode current and beam currents are shown in Figure 14-right. Due to their small impact on studies related to the collision frequencies the Xe^{+++} have been

excluded from these simulations. The singly- and doubly-charged ion beam currents are $I^+=13.7$ A and $I^{++}=4.6$ A. The computed profile for T_e appears to be in fair agreement with the measurements as suggested by Figure 15-right (solid curve).

The dashed curves in Figure 14 illustrate the corresponding results when v_B , Ω_e and all other plasma variables are determined self-consistently with no spatial restrictions on α in the far-plume. The motivation for these simulations is not to imply that anomalous (Bohm) diffusion extends to the far-plume; here we aim to demonstrate the effect that the *ad-hoc* elimination of the Bohm collision rate and Hall parameter has on the plasma solution. The proposed implication is that in models such as HPHall the inherent limitations posed by the quasi-1D assumption on the extent of the computational domain make the achievement of a numerical solution that is unbiased by the imposed restrictions beyond the near-cathode line (see Figure 6) challenging if not impossible. The relatively small differences between the two simulation cases for the the integrated variables such as anode and beam currents (see Figure 14-right) falsely imply a small effect by the imposed restrictions. But the comparisons for the electron temperature do not support such assertions. Figure 15-right quantifies the different spatial extents associated with the diffusion of heat in the electron flow along the channel midline for the two cases, and Figure 16 compares the 2-D profiles.

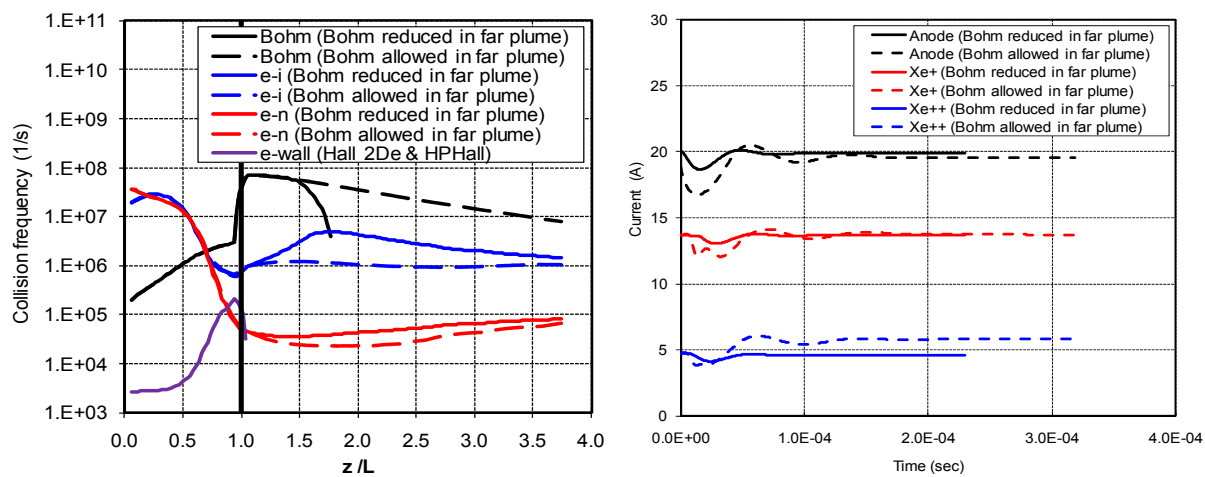


Figure 14. Studies on the effect of reducing the Bohm collision rate and the Hall parameter in the far plume (case shown is for the maximum Bohm factor $\alpha=0.4$). Left: Collision frequencies along the middle of the channel. Right: Anode and beam currents as a function of numerical simulation time.

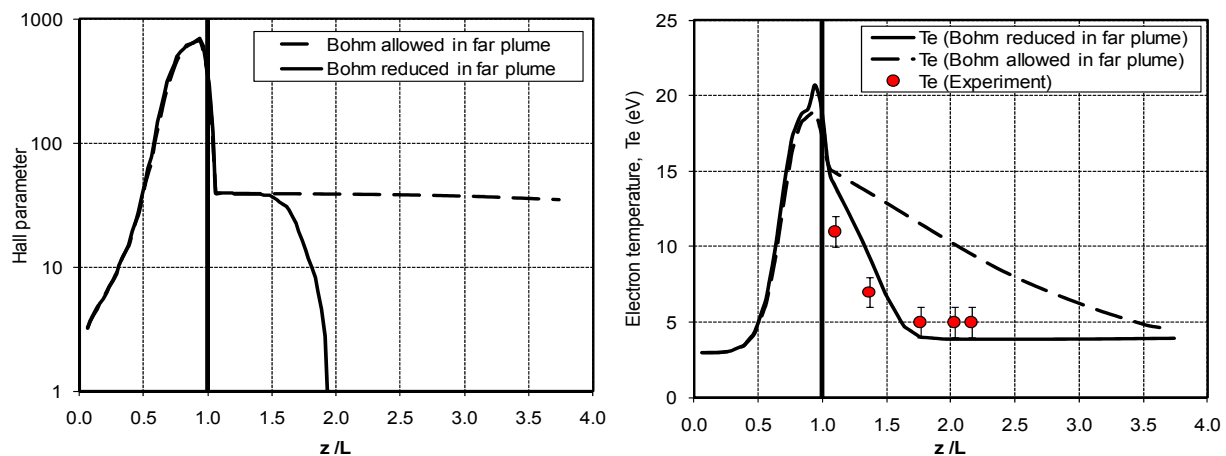


Figure 15. Studies on the effect of reducing the Bohm collision rate and the Hall parameter in the far plume (case shown is for the maximum Bohm factor $\alpha=0.4$). The plots compare solutions along the middle of the channel.

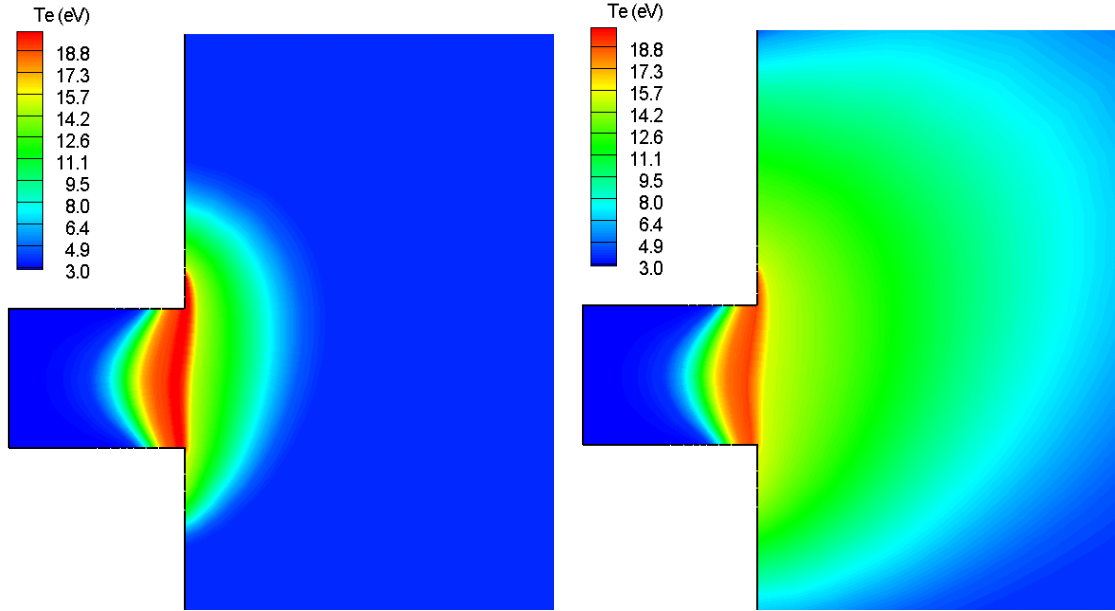


Figure 16. Studies on the effect of reducing the Bohm collision rate and the Hall parameter in the far plume (case shown is for the maximum Bohm factor $\alpha=0.4$). The plots compare 2-D contours of the electron temperature. Left: ν_B and Ω_e reduced beyond $z/L \sim 1.5$. Right: No reductions of ν_B and Ω_e in the far plume.

A related result is in Figure 17, which shows 2-D contours of the Hall parameter overlaid by unit vectors of the electron flux for the case of no reductions of α in the far-plume region. Selected streamlines of the magnetic field are also shown. The plot suggests the formation of an effective funneling region for the electrons that extends far beyond the end of the HPHall computational region. The regions of lowest Hall parameter are closely aligned with the ion beam as shown in Figure 17-right; this is where the drag force density \mathbf{R}_e on the electrons has the largest contributions by the classical e-i collision rate. However, because the Bohm collision for this case (of maximum $\alpha=0.4$) remains the dominant rate throughout the plume region the precise electron paths, especially in the areas near the magnets (i.e. the “lobes” of high Hall parameter shown in Figure 17) cannot yet be identified.

The proximity of the values of the two collision frequencies, e-i and Bohm, in the far-plume regions and the apparent insignificance of the Bohm collision rate in most of the acceleration channel motivated the next series of numerical simulations. In these simulations we aim to eliminate the Bohm collision rate inside the channel while lowering the value of α in the plume even further. Two cases are compared in Figure 18-left and Figure 19-left for the maximum value of the Bohm factor: $\alpha=0.15$ and $\alpha=0.075$. The Bohm collision rate inside the channel for both cases has been eliminated as shown in Figure 19-left. The comparison with plasma measurements for the case of $\alpha=0.15$ is shown Figure 19-right. As in the BPT-4000 cases, it is found that by reducing the ν_B in the plume region the damping of the low-frequency oscillations is also diminished. Figure 18-right shows oscillations in the computed currents with a frequency of ~ 8.5 kHz, which is about 2.5 times lower than the observed value of ~ 20 kHz. The average anode current in both cases is also lower than the observed value by ~ 3.5 A. These simulations combined with the previous results illustrate the dependence of the spatial and temporal parts of the solution on the magnitude and spatial distribution of the Bohm collision rate. The α -trends from all the preliminary simulations that have been presented in this paper suggest that lowering α even further may increase the amplitude of the low-frequency oscillations but the effect on the time-averaged currents is not yet known. Also, Figure 17-left suggests that lowering α further could have a significant effect on the funneling of electrons from the plume regions, especially in relation to the expected increase of the Hall parameter near the magnets and the diffusion of electrons in these regions. Further studies on α , extended comparisons with time-averaged plasma measurements and predictions of thruster performance have not yet been performed but are planned as part of the development and validation of Hall 2De.

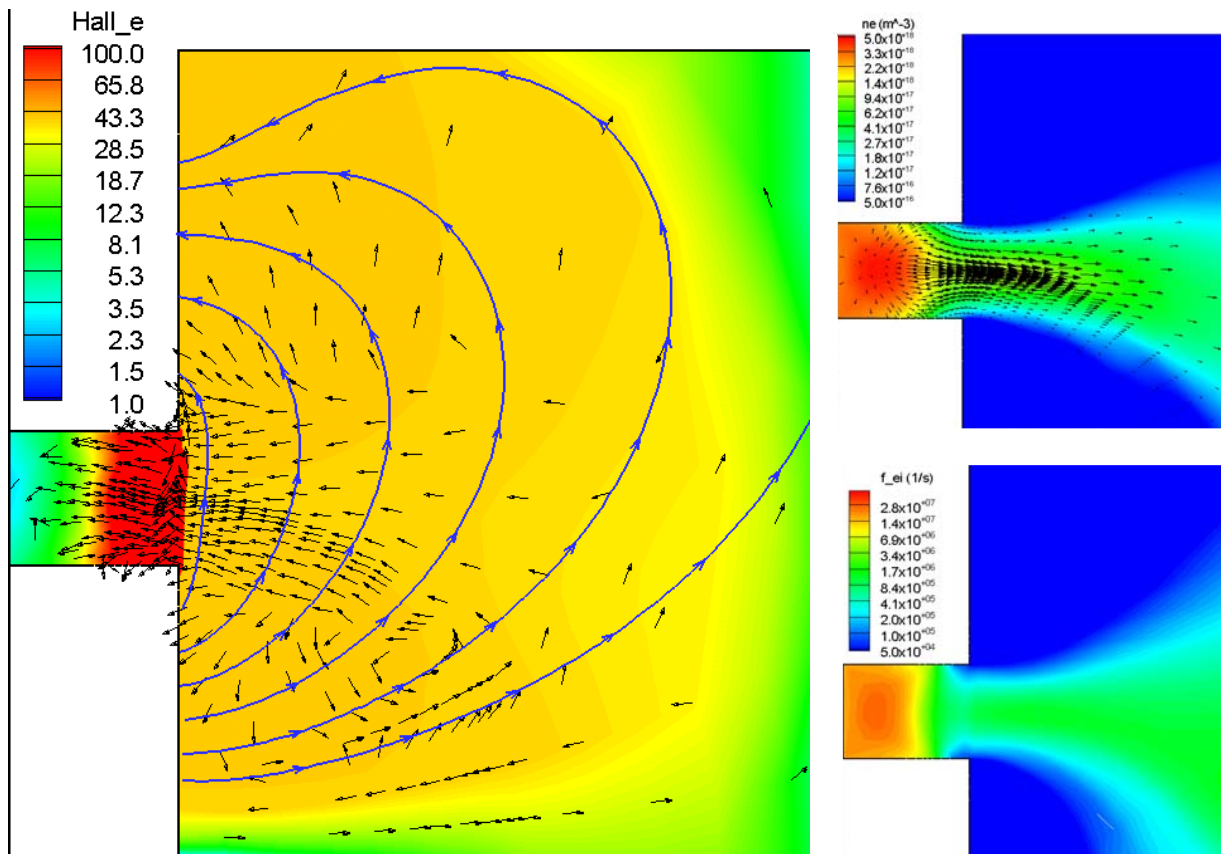


Figure 17. Left: contours of the Hall parameter overlaid by unit vectors of the electron particle flux and by selected streamlines of the magnetic field (shown in blue). Right-top: contours of the electron number density overlaid by the singly-charged ion velocity field. Right-bottom: contours of the e-i collision rate.

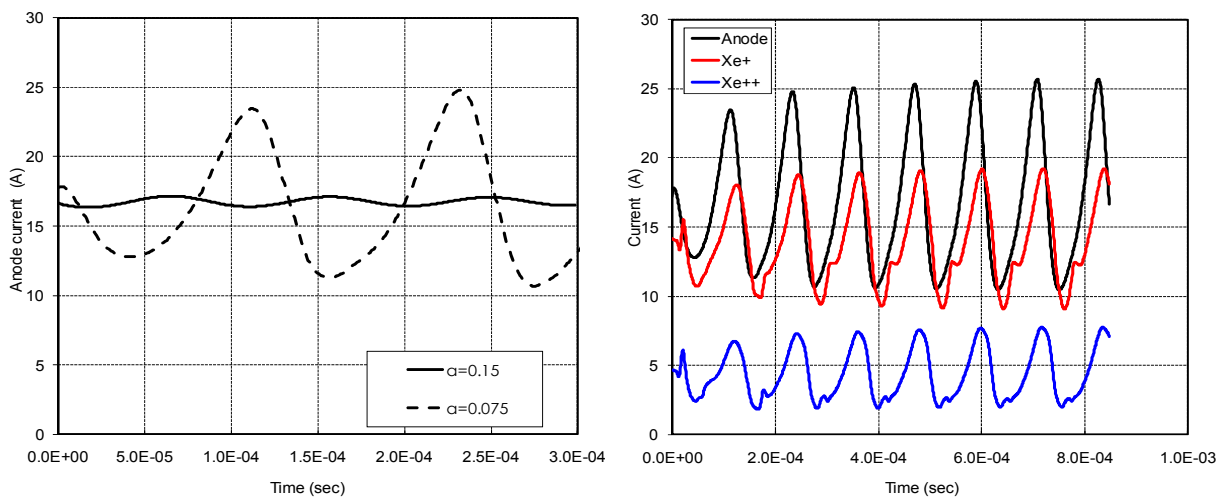


Figure 18. Numerical simulations of the 6 kW Hall thruster with no Bohm diffusion inside the acceleration channel. Left: anode current for two values of α : 0.15 and 0.075. Right: anode and beam currents for $\alpha = 0.075$ (longer simulation time).

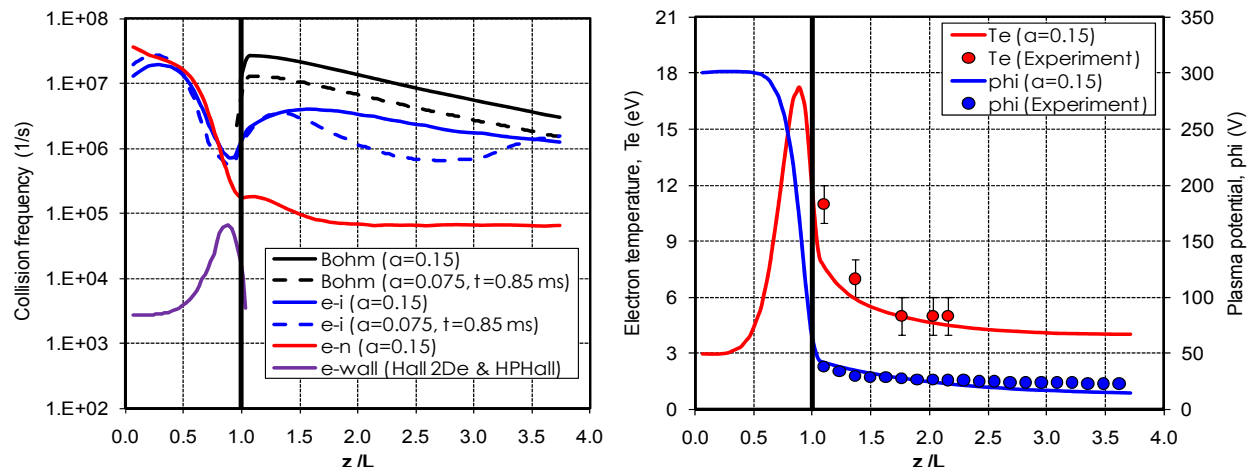


Figure 19. Numerical simulations of the 6 kW Hall thruster with no Bohm diffusion inside the acceleration channel. Left: collision frequencies (e-i and Bohm are compared for two values of α : 0.15 and 0.075). Right: comparisons for the case of $\alpha=0.15$ with plasma measurements along the middle of the acceleration channel.

IV. Conclusion

This paper reported on the development of a 2-D axisymmetric computational model for Hall thrusters that has the following main features: (1) resolution of electron transport both in parallel and perpendicular to the magnetic field, made possible by the discretization of the electron fluid equations on a field-aligned mesh, (2) implicit solution for the conduction of electron current and heat, (3) large computational region (by comparison to state-of-the-art hybrid simulation models) that extends several times the channel size downstream of the thruster exit, (4) solution of the hydrodynamic equations of continuity and momentum for isothermal ions, accounting for multiple ionization and charge-exchange collisions with neutrals, (5) an algorithm for the (collisionless) neutral gas that does not depend on discrete particles and is therefore free of statistical noise.

A set of preliminary simulations of the BPT-4000 and of a 6 kW laboratory Hall thruster suggest that the anode region is dominated by ion diffusion with the electric field predicted to be negligibly small there. The results show a significantly higher plasma density in this region by comparison to the hybrid simulation results of HPHall. Studies to assess the importance of the Bohm collision rate (that is usually imposed in the HPHall simulations) on the spatial and temporal behavior of the plasma suggest that the solution is not insensitive to the conditions imposed beyond the near-cathode magnetic field line. Although it has been known (at least for the two thrusters studied here) that the imposed spatial distribution of the Bohm collision rate in HPHall has a significant effect on the plasma solution in the vicinity of the channel exit, the significance of the conditions imposed downstream of the near-cathode streamline could not be assessed due, in part, to the limited extent of the HPHall domain. By solving for the electron flow with the Hall 2De extended region it is found that the flow field exhibits characteristics that are purely two-dimensional and cannot be resolved with a quasi-one-dimensional electron model. In regards to the temporal behavior of the solution it is found that the Bohm collision rate also influences significantly the damping of the current oscillations. If lowered sufficiently, to values that begin to near the e-i collision rate in regions of the plume, only then does the plasma begin to exhibit the temporal behavior that is known to persist in Hall thrusters (the well-known “breathing mode”). Although the questions on turbulence and its significance on the transport of electrons remain unanswered by the simulation results presented herein, it appears that the path to the answer cannot exclude the two-dimensional character of the electron flow field in the thruster plume.

Acknowledgments

The research described in this paper was carried out by the Jet Propulsion Laboratory, California Institute of Technology, under a contract with the National Aeronautics and Space Administration. Reference herein to any specific commercial product, process, or service by trade name, trademark, manufacturer, or otherwise, does not constitute or imply its endorsement by the United States Government or the Jet Propulsion Laboratory, California Institute of Technology.

References – to be formatted

- ¹ Morozov, A. I., Plasma Accelerators, ed. Archimovich L. A., M. Mashinostroenie , 1973, p. 5-15, 85-92 (in Russian).
- ² Morozov, A. I., Melikov I. V., Journal of Technical Physics, 1974, v. 44, No. 3, p. 544 (in Russian).
- ³ Volkov, B. I., Morozov A. I., Sveshnikov A. G., Yakunin C. A., preprint Kurchatov Inst. Atomic Energy, No. 2945, M. 1978 (in Russian).
- ⁴ M. Hirakawa and Y. Arakawa. Particle simulation of plasma phenomena in Hall thrusters. In Proc. 24th International Electric Propulsion Conference, number 95-164, Moscow, 1995.
- ⁵ M. Hirakawa and Y. Arakawa. Numerical simulation of plasma particle behavior in a Hall thruster. In Proc. 32nd AIAA Joint Propulsion Conference, number 96-3195, Lake Buena Vista, 1996.
- ⁶ M. Hirakawa. Electron transport mechanism in a Hall thruster. In Proc. 25th International Electric Propulsion Conference, number 97-021, Cleveland, 1997
- ⁷ Fife, J. M., "Hybrid-PIC Modeling and Electrostatic Probe Survey of Hall Thrusters," Ph.D. Thesis, Aeronautics and Astronautics, Massachusetts Institute of Technology, 1998
- ⁸ Fife, J. M., Martinez-Sanchez, M., and Szabo, J., "A Numerical Study of Low-Frequency Discharge Oscillations in Hall Thrusters," 33rd AIAA/ASMA/SAE/ASEE Joint Propulsion Conference, Seattle, Washington, July 1997.
- ⁹ Bohm, D., Burhop, E.H.S., and Massey, H.S.W., in \Characteristics of Electrical Discharges in Magnetic Fields," A. Guthrie and R. K. Waterling, Eds., McGraw-Hill, New York, 1949.
- ¹⁰ Parra, F. I., Ahedo, E., Fife, J. M., and Martinez-Sanchez, M., "A Two-Dimensional Hybrid Model of the Hall Thruster Discharge," Journal of Applied Physics 100, 023304 (2006).
- ¹¹ Gamero-Castaño, M. and Ziemer, J. < Estimation of Hall thruster erosion using HPHall, < 29th International Electric Propulsion Conference, Princeton, USA
- ¹² Hofer, R. R., Mikellides, I. G., Katz, I., and Goebel, D. M., "BPT-4000 Hall Thruster Discharge Chamber Erosion Model Comparison with Qualification Life Test Data," Presented at the 30th International Electric Propulsion Conference, IEPC Paper 2007-267, Florence, Italy, Sept. 17-20, 2007.
- ¹³ Efficacy of Electron Mobility Models in Hybrid-PIC Hall Thruster Simulations, Richard R. Hofer, Ira Katz, Ioannis G. Mikellides, Dan M. Goebel, Kristina K. Jameson, Regina M. Sullivan, and Lee K. Johnson Jet Propulsion Laboratory, California Institute of Technology, Pasadena, CA 91109 AIAA-2008-4924 R05.doc
- ¹⁴ E. Fernandez, M. A. Cappelli, and K. Mahesh, "2-D simulations of Hall thrusters," in *CTR Annual Research Briefs*. Palo Alto, CA: Stanford Univ., 1998, p. 81.
- ¹⁵ IEEE TRANSACTIONS ON PLASMA SCIENCE, VOL. 35, NO. 5, OCTOBER 2007 1379 Simulating Plasma-Induced Hall Thruster Wall Erosion With a Two-Dimensional Hybrid Model Emmanuelle Sommier, Michelle K. Scharfe, Nicolas Gascon, Mark A. Cappelli, and Eduardo Fernandez
- ¹⁶ G. J. M. Hagelaar, J. Bareilles, L. Garrigues, and J. P. Boeuf, *J. Appl. Phys.* **91**, 5592 ~2002!
- ¹⁷ Critical assessment of a two-dimensional hybrid Hall thruster model: Comparisons with experiments J. Bareilles, G. J. M. Hagelaar, L. Garrigues, C. Boniface, and J. P. Boeuf) Centre de Physique des Plasmas et Applications, Université Paul Sabatier, 118 Route de Narbonne, 31062 Toulouse Cedex 4, France N. Gascon) PHYSICS OF PLASMAS VOLUME 11, NUMBER 6 JUNE 2004
- ¹⁸ Morozov, A. I. and Savelyev, V. V., "Numerical Simulation of Plasma Flow Dynamics in SPT", IEPC 1995, 161.
- ¹⁹ A. I. Morozov and V. V. Savelyev, "Fundamentals of stationary plasma thruster theory," *Rev. Plasma Phys.*, vol. 21, p. 203, 2000.
- ²⁰ Plasma flow and plasma-wall transition in Hall thruster channel, M. Keidara) and I. D. Boyd Department of Aerospace Engineering, University of Michigan, Ann Arbor, Michigan 48109 I. I. Beilis Electrical Discharge and Plasma Laboratory, Fleischman Faculty of Engineering, Tel Aviv University, P. O. Box 39040, Tel Aviv 69978, Israel
- ²¹ Mikellides, I. G., Katz, I., Goebel, D. M., Jameson, K. K., and Polk, J. E., "Wear Mechanisms in Electron Sources for Ion Propulsion, II: Discharge Hollow Cathode," *J. Prop. Power*, Vol. 24, No. 4, 2008, pp. 866-879.
- ²² Mikellides, I. G., and Katz, I., "Wear Mechanisms in Electron Sources for Ion Propulsion, I: Neutralizer Hollow Cathode," *J. Prop. Power*, Vol. 24, No. 4, 2008, pp. 855-865.
- ²³ Wirz R. E., "Discharge Plasma Processes of Ring-Cusp Ion Thrusters," Ph.D. Dissertation, Aeronautics, Caltech, Pasadena, CA, 2005.

- ²⁴ "A New Algorithm for the Neutral Gas in the Free-Molecule Regimes of Hall and Ion Thrusters, IEPC-2009-95, Ira Katz and Ioannis G. Mikellides.
- ²⁵ Laser-Induced Fluorescence of Singly-Charged Xenon inside a 6-kW Hall Thruster, Wensheng Huang *, Brittany Drenkow†, and Alec D. Gallimore‡, 45th AIAA/ASME/SAE/ASEE Joint Propulsion Conference & Exhibit 2 - 5 August 2009, Denver, Colorado, AIAA 2009-5355. Plasmadynamics and Electric Propulsion Laboratory, University of Michigan, Ann Arbor, MI 48109
- ²⁶ Miller et. al., J. Appl. Phys., Vol. 91, No. 3, 1 February 2002
- ²⁷ Zumdahl, S., *Chemistry*, D. C. Heath & Co., 1986, pg. 280.
- ²⁸ Reid, B. M. and Gallimore, A. D., "Langmuir Probe Measurements in the Discharge Channel of a 6-kW Hall Thruster," AIAA Paper 2008-4920, July 2008.
- ²⁹ Hobbs, G. D. and Wesson, J. A., "Heat Flow through a Langmuir Sheath in the Presence of Electron Emission," *Plasma Physics* 9, 85-87 (1967).
- ³⁰ Hofer, R. R., Mikellides, I. G., Katz, I., and Goebel, D. M., "Wall Sheath and Electron Mobility Modeling in Hybrid-PIC Hall Thruster Simulations," AIAA Paper 2007-5267, July 2007.
- ³¹ The Influence of Neutral Flow Rate in the Operation of Hall Thrusters, Ph.D. Thesis, Aerospace Engineering, University of Michigan, 2009 by Bryan Michael Reid
- ³² Private conversations with Dan Goebel. Data not yet published.
- ³³ Brown, D. L., Larson, C. W., Haas, J. M., and Gallimore, A. D., "Analytical Extraction of Plasma Properties Using a Hall Thruster Efficiency Architecture," IEPC Paper 2007-188, Sept. 2007.
- ³⁴ Shastry, R., Hofer, R. R., Reid, B. M., and Gallimore, A. D., "Method for Analyzing ExB Probe Spectra from Hall Thruster Plumes," AIAA Paper 2008-4647, July 2008.
- ³⁵ Jameson, K. K., "Investigation of Hollow Cathode Effects on Total Thruster Efficiency in a 6 kW Hall Thruster," Ph.D. Dissertation, Aerospace Engineering, University of California, Los Angeles, 2008.